UNIVERSIDADE FEDERAL DO ESPÍRITO SANTO
CENTER OF EXACT SCIENCES
POSTGRADUATE PROGRAM IN PHYSICS

Master's Dissertation

A Theoretical Study of Samarium Hexaboride (SmB_6) as a Possible Candidate for Light Dark Matter (LDM) Direct Detection

Thiago Dias Loyola

Vitória
2023

Thiago Dias Loyola

A Theoretical Study of Samarium Hexaboride (SmB_6) as a Possible Candidate for Light Dark Matter (LDM) Direct Detection

Dissertation presented to the Postgraduate Program in Physics at the Center of Exact Sciences of the Universidade Federal do Espírito Santo as a partial requirement for obtaining the Master's degree in Physics in the area of Condensed Matter Physics.

Advisor: Prof. Dr. Wendel Silva Paz

Vitória
2023

Ficha catalográfica disponibilizada pelo Sistema Integrado de Bibliotecas - SIBI/UFES e elaborada pelo autor

---

Loyola, Thiago Dias, 1995-
L923t A Theoretical Study of Samarium Hexaboride (SmB6) as a Possible Candidate for Light Dark Matter (LDM) Direct Detection / Thiago Dias Loyola. - 2023.
97 f.

Orientador: Wendel Silva Paz.
Dissertação (Mestrado em Física) - Universidade Federal do Espírito Santo, Centro de Ciências Exatas.

1. Matéria escura leve. 2. Física do estado sólido. 3. Detecção de partículas. 4. DFT. 5. Materiais topológicos. 6. Hexaboreto de Samário. I. Paz, Wendel Silva. II. Universidade Federal do Espírito Santo. Centro de Ciências Exatas. III. Título.

CDU: 53

UNIVERSIDADE FEDERAL DO ESPÍRITO SANTO
CENTRO DE CIÊNCIAS EXATAS
PROGRAMA DE PÓS-GRADUAÇÃO EM FÍSICA

"A Theoretical Study of Samarium Hexaboride (SmB6) as a Possible Candidate for Light Dark Matter (LDM) Direct Detection"

Thiago Dias Loyola

Dissertação submetida ao Programa de Pós-Graduação em Física da Universidade Federal do Espírito Santo, como requisito parcial para a obtenção do título de Mestre em Física.

Aprovada por:

Prof. Dr. Wendel Silva Paz
(Orientador-PPGFis)

Prof. Dr. Tales Costa de Freitas
(IFES-Linhares)

Prof. Dr. Wesley Spalenza
(IFES-Cariacica)

Prof. Dr. Humberto Belich Junior
(PPGFis/UFES)

Vitória-ES, 22 de dezembro de 2023

AGRADECIMENTOS

Agradeço inicialmente aos meus pais, Adilson e Angela, por todo apoio e suporte que me foi dado e por estarem sempre me encorajando a seguir em frente. Para além deles, agradeço também aos meus amigos, Kássio e José Carlos, e a minha companheira, Suellen. Agradeço também aos meus colegas de curso, em especial ao Nathanael e à Marcella, pelas reflexões, pelo suporte e pelos ensinamentos. Decerto carregarei sempre um pouco de todos vocês comigo.

Agradeço também aos membros da banca por terem aceito o convite e à Universidade Federal do Espírito Santo por ter disponibilizado um espaço tão belo e confortável para que eu desse continuidade aos meus estudos. Por fim, agradeço ao meu orientador pela orientação e apoio.

Por último, e não menos importante, agradeço ao Conselho Nacional de Desenvolvimento Científico e Tecnológico (CNPq) e à Fundação de Amparo à Pesquisa e Inovação do Espírito Santo (FAPES) pela confiança e pelo suporte financeiro.

"Tell me and I forget, teach me and I may remember, involve me and I learn."

Xun Kuang

ABSTRACT

The mystery surrounding the existence of dark matter, prompted by a substantial mismatch between theoretical predictions and experimental observations in galaxies and galaxy clusters, remains a formidable mystery awaiting resolution. A pivotal aspect of unraveling this mystery lies in its detection. It is crucial to note that this persistent enigma has led us to the formulation of different models detailing its composition and interactions with ordinary matter.

In the scope of the present study, our focus centers on Light Dark Matter (LDM). Furthermore, we operate under the assumption that its interactions occur through a dark photon that is transformed into a visible photon and absorbed during the interaction process. In the subsequent discussion on the direct detection of new particles using a target, our primary objective revolves around quantifying parameters intricately linked to the interaction between the particle and the target. It is still crucial to emphasize that the nature of the target may lead us down distinct avenues within the realm of physics since molecule targets and crystal targets are analyzed by different approximations, boundary conditions, and symmetries. However, the quest for heightened interaction probability steers us inevitably into the domain of Material Science, where the size of the target becomes a pivotal determinant of success.

In the context of the light-dark matter, the material selected must meet some specific criteria, including scalability, band gap, Fermi velocity, and topology, and these stand for the points that will guide us through all subsequent development up to the positive conclusion concerning the use of Samarium Hexaboride (SmB_6) as a target in this detection process.

Keywords:

Condensed Matter Physics, Material Science, Crystals, Lattice, Band Structure, Band Theory, Fermi-Dirac distribution, Dark Matter, Light Dark Matter, Direct Detection, Detection of Particles, Samarium Hexaboride, SmB6.

RESUMO

O mistério em torno da existência da matéria escura, desencadeado por uma discrepância substancial entre previsões teóricas e observações experimentais em galáxias e aglomerados de galáxias, permanece um enigma que aguarda resolução. Por outro lado, uma abordagem prática e fundamental que desvendaria essa questão, ou parte dela, de uma vez por todas, consistiria na sua detecção. É crucial observar ainda que tal mistério levou à formulação de diferentes modelos detalhando a sua composição e possível interação com a matéria ordinária.

No escopo do atual estudo, o nosso foco se concentra na Matéria Escura Leve (LDM). Além disso, trabalhamos com a suposição de que as suas interações ocorrem por meio de um fóton escuro, que é transformado em um fóton claro e absorvido durante o processo de interação.

Na discussão subsequente à detecção direta de novas partículas através da utilização de um alvo, o nosso objetivo principal girará em torno da quantificação de parâmetros intrinsecamente ligados à interação entre a partícula e o alvo propriamente dito. É crucial enfatizar ainda que a natureza do alvo escolhido pode nos conduzir por caminhos distintos dentro do domínio da física, uma vez que alvos moleculares e cristalinos são analisados por diferentes aproximações, condições de contorno, e simetrias. Entretanto, no nosso caso, a busca por uma probabilidade de interação mais elevada nos conduz inevitavelmente ao domínio da Ciência dos Materiais, onde o tamanho do alvo torna-se um determinante crucial de sucesso.

No contexto da matéria escura leve, o material selecionado deve atender a critérios específicos, incluindo escalabilidade, intervalo de banda, velocidade de Fermi e topologia, e estes representam os pontos que nos guiarão por todo o desenvolvimento subsequente até a conclusão positiva sobre o uso do Hexaboreto de Samário (SmB_6) como alvo nesse processo de detecção.

Palavras-chave:

Física da Matéria Condensada, Ciência dos Materiais, Cristais, Redes Cistalinas, Estrutura de Bandas, Teoria de Bandas, Distribuição de Fermi-Dirac, Matéria Escura, Matéria Escura Leve, Detecção Direta, Detecção de Partículas, Hexaboreto de Samário, SmB6.

List of Figures

List of Tables

Contents

Chapter 1

Introduction

The existence of dark matter, although it is predicted for galaxies and galaxy clusters due to a massive discrepancy between theoretical and experimental data [1], is still a mystery to be solved, and part of the solution process falls into its detection. At this point, it is worth noting that we have different models for its composition and interaction with ordinary matter [36]. In the current work, we are interested in Light Dark Matter (LDM), plus we are assuming that its interaction takes place through a dark photon that is turned into a bright photon and absorbed afterward during the interaction process.

In what follows, as far as we are considering detecting new particles directly with a target, we aim all of our efforts at measuring greatnesses that are notably related to the interaction between the particle with our target [30]. At this point, it is noteworthy that we could think of two different kinds of targets that would subsequently lead us to different areas in Physics, they are molecules and crystals. On the other hand, since we are looking for ways to increase the interaction probability, the larger our target is, the better it is, and, consequently, we inevitably fall into the Material science domain. Regarding light-dark matter, this material should still satisfy some specific properties, such as band gap, Fermi velocity, and topology [20, 24, 49]. Chart 1.1 summarizes this brainstorm up to Samarium Hexaboride (SmB_6), the material we are proposing as a possible target here.

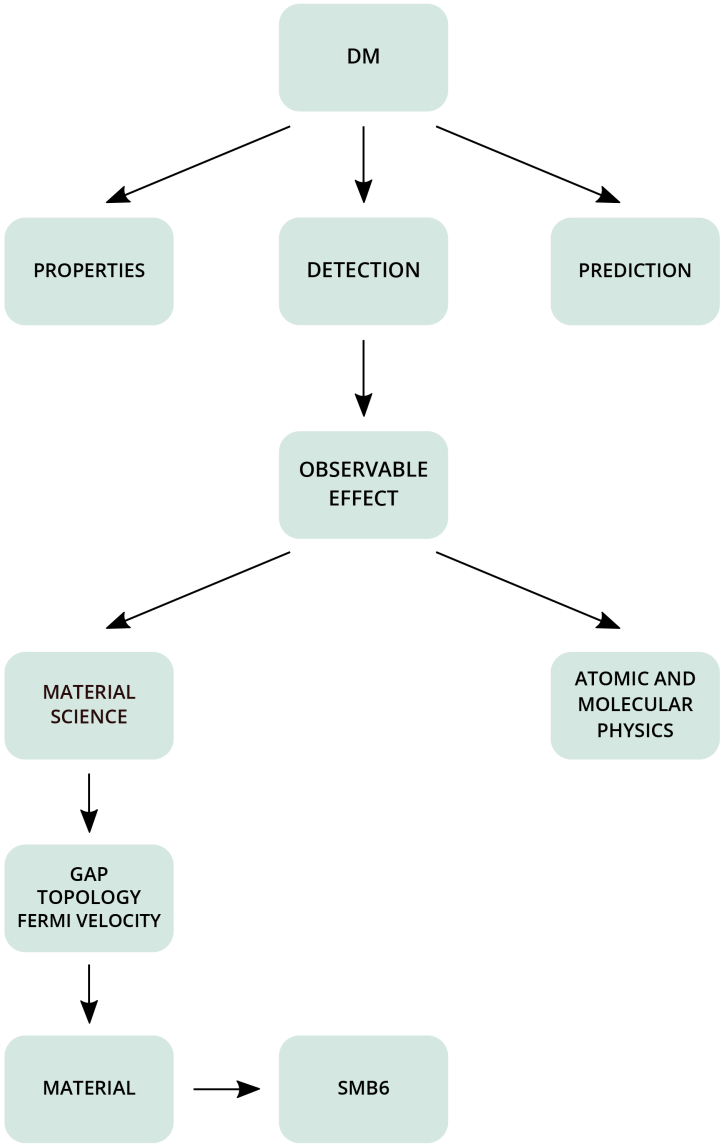

Figure 1.1. Fluxogram that depicts the reasoning process from conceiving dark matter up to proposing a target to be employed at its direct detection process.

The upcoming chapters are all going to be developed upon the necessary concepts to give the reader a solid base to understand the main ideas presented in this work, the results, and how to link them. First, we are going to discuss what is dark matter, when it was predicted, and how we can possibly detect it directly. Then, since we fall into the material science domain, we are going

to develop all the concepts necessary to understand the detection process. Afterward, we will discuss and develop the main numerical methods employed here, while our main input is shown in a separate appendix. Finally, in the final chapters, you can find the results, a brief discussion about them, and our conclusion.

Chapter 2

Overview

In this chapter, we are going to skim over some basic but important and necessary concepts that the reader should bear in mind before jumping to the results. In short, we will address the following questions: what is dark matter? What are its types? How could we possibly detect it directly? What are crystals, and why are they important to the current work?

2.1 Dark Matter

The evidence of dark matter is settled upon the difference between the observable and the predicted gravitational masses of galaxies, which indicates the presence of a huge unseen mass in the Universe, otherwise, the whole system would be physically infeasible.

To understand what the so-called dark matter stands for, we begin our journey by settling down an important concept. First, we've got to address the question of what is a gravitational mass, and why it does play an important role in understanding dark matter. Then, we will quickly handle the issue of why it is called dark matter and how it is distinguished from the usual mass.

At this point, note that the concept of mass first arises from Newton's laws. Despite that, if we look back on all his laws, we may promptly notice the existence of not only one, but two different masses, one in the second law, and the other in the gravitational law, given by [53]:

$$\mathbf{F} = m_i \mathbf{a} \qquad , \qquad \mathbf{F} = m \frac{GM}{|\mathbf{r} - \mathbf{r}'|} \hat{\mathbf{r}} \approx m_g \mathbf{g} \tag{2.1}$$

where the subscripts i, and g denote **i**nertial, and **g**ravitational, respectively. Despite that, we have known ever since Newton that they are both equal, but nobody had been able to answer this question precisely for more than 200 years until Einstein[1]. Therefore, we find no difficulties in addressing the first question with the standard interpretation of mass, which relates it to the natural resistance of a body to any changes in its movement. It is worth noting, though, that mass and matter, in what concerns the current discussion, stand for the same thing, a bunch of particles. Consequently, dark matter, or simply dark mass, is made of a set of yet unknown particles that maintain the universe. This prompts us to delve into the subsequent questions: What precisely are these particles? Why is the term "dark" employed? Where is dark matter situated, and how can we detect its presence?

2.1.1 First Predictions

The main implication of the gravitational law is that we can always measure a force of attraction between masses of any kind. Therefore, if we leave a bunch of particles with a zero net electric charge at rest in space, they will inevitably be drawn together, gradually closing the gap between them. To avoid this *disaster* in what concerns stellar systems, the only option we have left is that they must be moving neither towards nor far away, but around each other as Kepler stated in the early seventeenth century for the solar system [53]. It may be schematically shown by:

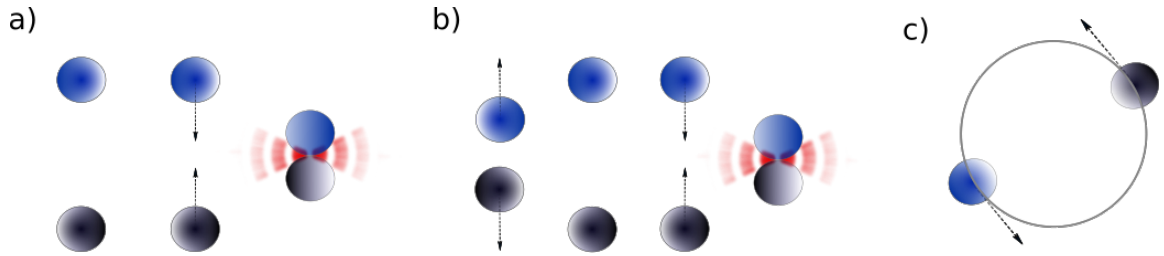

Figure 2.1. a) Here, the particles are initially at rest. If that's the case, then they instantly start moving towards their common center and eventually crash into each other. b) If the bodies are initially moving far away with a speed that is smaller than escape velocity, then they will eventually stop and start moving towards their common center as depicted in (a). c) Here the particles are moving around the common center, instead. That stands for the only stable solution for a two-particle system in a dynamical equilibrium.

[1] A further discussion is found in [11].

Then, if we keep that in mind, and recall that our main intention here is to find the gravitational mass of far objects, we can safely jump to conclusions and say that we have just depicted a simple method to measure it. In other words, we first study their movements and use all the gathered information to predict the necessary mass to keep the system bonded. For example, the average motion of a star in a spiral galaxy, such as the one in the figure below:

Figure 2.2. Visible light Hubble data combined with infrared data from Spitzer, went into creating this stunning image of M51, also known as Whirlpool galaxy. M51, as we can see, is two interacting galaxies (formally NGC 5194 and 5195), where there left-most one is an example of the aforementioned spiral galaxy. Image taken from [41].

takes on an approximately circular form, enabling us to search for a circular velocity that precisely counterbalances its orbital motion around the galactic center. Despite that, when we do it and face our results with experimental data, we promptly notice a big difference between the predicted and the observed gravitational masses. Consequently, since all laws we have discussed so far are expected to be right, this difference can only be due to an unseen mass that is hidden somewhere in the galaxy and which does play an essential role in the maintenance of the system's stability. The most remarkable difference between the standard gravitational mass and this one yet unknown

comes from the fact that it can't be seen because its particles don't interact electromagnetically with light. Therefore, especially due to this fact, it is known as dark matter, while the ordinary gravitational mass is called luminous matter [36]. In the upcoming sections, we are skimming over some of its properties, when it was predicted, and how we can possibly detect it directly.

Spiral Galaxies

In the early study of spiral galaxies, we used to expect to find a high-density bulge at their centers. Such a bulge would provide the necessary consistency for the whole system as aforementioned. So, since all stars are moving around the galactic center with a circular velocity $v(r)$ that is counterbalanced by a centrifugal force, we know, from classical mechanics, that [53]:

$$\frac{mv^2}{r} = \frac{GmM_{<r}}{r^2} \tag{2.2}$$

where v is the star's speed, m is its mass, r its position, and $M_{<r}$ is the mass enclosed within the radius r. Consequently, if we are out of the bulge, M becomes constant, and we get:

$$\frac{\cancel{m}v^2}{\cancel{r}} = \frac{G\cancel{m}M_{<r}}{r\cancel{^2}} \implies v^2 = \frac{GM}{r} \implies v(r) \propto \frac{1}{\sqrt{r}} \tag{2.3}$$

On the other hand, if such a star is within the high-density region, and we assume such a density to be approximately constant, we find:

$$\frac{mv^2}{r} = \frac{GmM_{<r}}{r^2} \implies \frac{mv^2}{r} = \frac{Gm}{r^2}\frac{4}{3}\pi r^3\rho \implies \frac{v^2}{r} = \frac{4}{3}G\pi\rho r \implies v(r) \propto r \tag{2.4}$$

Surprisingly enough, this behavior is just partially found in measurements as can be seen in figure 2.3. Despite that, if we look back on equation 2.2, we promptly realize that v is constant if, and only if, $M_{>r} \propto r$, which suggests the presence of an enormous unseen mass in the galaxy, which would be the dark matter [36].

Galaxy Clusters

As galaxies, galaxy clusters, namely a set of galaxies bonded by a common gravitational potential, are also on the Dark Matter way and their study follows a quite similar reasoning as

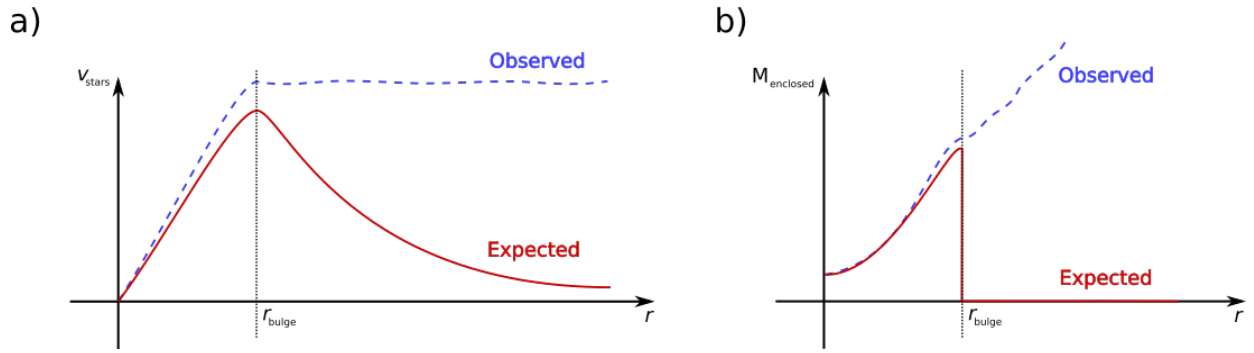

Figure 2.3. a) Stars' velocities do get higher in spiral galaxies as we approach the border of the bulge according to predicted, but observational measurements of rotation curves for several spiral galaxies show $v(r) \approx constant$ for larger r instead of the predicted proportion $r^{-1/2}$ [36]. b) Expected and observed masses for spiral galaxies.

the one aforementioned. The only difference here is that we no longer rely on eq. 2.2, but on the Virial Theorem instead, because we are now handling more than two particles. This theorem deals with non-relativistic interacting particles in dynamical equilibrium due to a central force and can be written as [36]:

$$V + 2K = 0 \tag{2.5}$$

where V and K are the system's total gravitational potential and kinetic energy, respectively. We can delve into this question a little further and consider the potential energy of a self-gravitating system, like a galaxy cluster, of mass M (density ρ), and radius R, from which we get [36]:

$$V = -\frac{3}{5}\frac{GM^2}{R} \tag{2.6}$$

and thus

$$-\frac{3}{5}\frac{GM^2}{R} + Mv_{rms}^2 = 0 \tag{2.7}$$

where v_{rms} is the root mean square of the velocity of each galaxy in the cluster. Consequently, if we know R, and v_{rms}, we can promptly estimate M [36].

Fritz Zwicky, in 1933, studied the movement of the galaxies within the Coma cluster, estimating then their masses. Surprisingly enough, he found out that the system's mass, in other to satisfy the observed medium-sized Doppler effect of 1000 km/s or more, should be at least 400 times greater than the one gotten through the luminous matter, and virial theorem [1]. He not

only considered galaxies in a dynamical equilibrium as we did here, nevertheless, he reached the same conclusion, which, for the first case, was, "If this should be verified, it would lead to the surprising result that dark matter exists in much greater density than luminous matter." (ZWICKY, 1933, p. 10).

2.1.2 Types of Dark Matter

Even though the precise nature of dark matter is yet unknown, one can classify it based on its possible production, its particles' nature, or even the mass of its particles. Nevertheless, since the current work is mainly focused on light-dark matter, we are only going to skim over the different categorizations and discuss a little further the mass one. Then, dark matter may be classified as follows [36]:

- **Thermal:** Dark matter can be classified according to whether it was produced thermally, denoted as thermal dark matter, or non-thermally;
- **Particle types:** It can also be of two distinct natures, baryonic, where the term "baryonic" encompasses not only baryons but all known particles, or non-baryonic;
- **Mass and speed:** Finally, depending on whether its particles are moving at relativistic speeds or not, one can classify it as Hot dark Matter, also known as light dark matter (LDM), or cold dark matter. While hot dark matter is generally made up of lighter particles moving at relativistic speeds, cold dark matter is generally composed of heavier, non-relativistic particles.

2.1.3 Detection of Particles

As long as we are talking about detecting new particles, it should be kept in mind that we are putting significant effort into measuring greatnesses that are notably related to the entity we are studying. Besides, depending on the scales we are in, for example, if the concerned energies are really small, external effects may need to be suppressed so observable effects get their deserved attention and we can safely make predictions. Regarding the process itself, it may still be direct, such as when we try to build up the particle in particle accelerators or to measure something out

of its interaction with a target, or indirect, when instead of looking closely at the particle, we put our efforts into measuring byproducts whose origin could only be due to the existence of the particle we are trying to detect. In short, we are constantly trying to measure something that can only be due to the existence of the particle [30]. The current work relies its development on direct detections, especially the ones involving a target. In this field, it is worth noting that we are mainly interested in measuring the recoil of nuclei due to the scattering of particles or the absorption of a photon with the subsequent optical transition. Finally, as pointed out previously, we could still think of two kinds of targets here, molecules or crystals, but since light-dark matter has very low cross-sections, we inevitably fall into the material science domain. We are then left with the following question: what properties should this material have to be used as a target? Regarding light-dark matter, this question will be properly addressed in the following section.

Direct Detection of Light Dark Matter

Although we don't know precisely the nature of dark matter, there are some models for its interaction with ordinary matter. The one we are considering supposes its interaction is provided by a dark photon that, yet we don't know how, is turned into a bright photon, which interacts with valence electrons pumping them up to the conduction band. This process may be depicted as follows [20, 24, 49]:

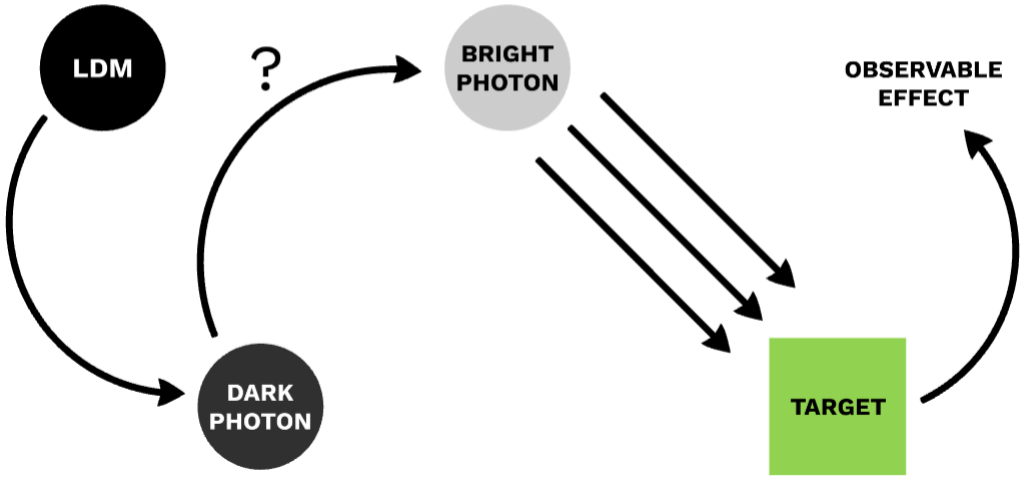

Figure 2.4. Adopted model for direct detection of LDM.

To measure an observable effect out of this interaction, though, our target must satisfy some properties, such as [20, 24, 49]:

- It must be scalable;
- It must be a semiconductor;
- Its Fermi velocity must be of the order of $10^{-3}\,c$;
- It must be a topological insulator;

At this point, we should bear in mind that these properties are all either, to increase the probability of interaction, or to diminish other effects. Regarding the properties themselves, we have that the material must be scalable due to the low probability of interaction involved in the process, and it must also be a semiconductor because of the energy of the involved bright photon, which is of the order of meV. Lastly, the requirement of a topological insulator comes from the following reasoning: the photon absorption will take place on the surface of the material, so if it is a topological insulator, then electrons of its bulk will pump up to its surface and reach protected states that will prevent them from suffering other undesired effects, such as scattering, while allowing us to direct measure an electrical current [20, 24].

We have only skimmed over all requirements concerning the current work so far, leaving further explanations to the upcoming sections. Consequently, the following sections will explain all that matters to reach a better understanding of what these greatnesses stand for and how we usually find them out.

2.2 Condensed Matter Physics

As pointed out previously, whenever we are working towards the direct detection of a yet unknown particle, we aim all of our efforts into measuring a variation out of the interaction of these particles with a well-known material. In short, if a system is isolated, and we measure a deviation in the properties of the material that was predicted numerically, then we may safely assign it to the presence of the particle under study. The main point here is: how large should this well-known material be? This question is properly addressed according to the interaction

probability, which in our case, due to the low numbers involved, falls into condensed matter physics and the crystal study. Consequently, in the upcoming sections, we are going to skim over this field and the main concepts handled in this work. At the moment, our first question is: what are crystals?

2.2.1 Crystals

One can classify materials in general according to their regularity, which is simply the presence or not of a high level of homogeneity[2]. If it does have it, then it is called crystalline, otherwise, it is denoted as amorphous. For clarity's sake, look at the following figure:

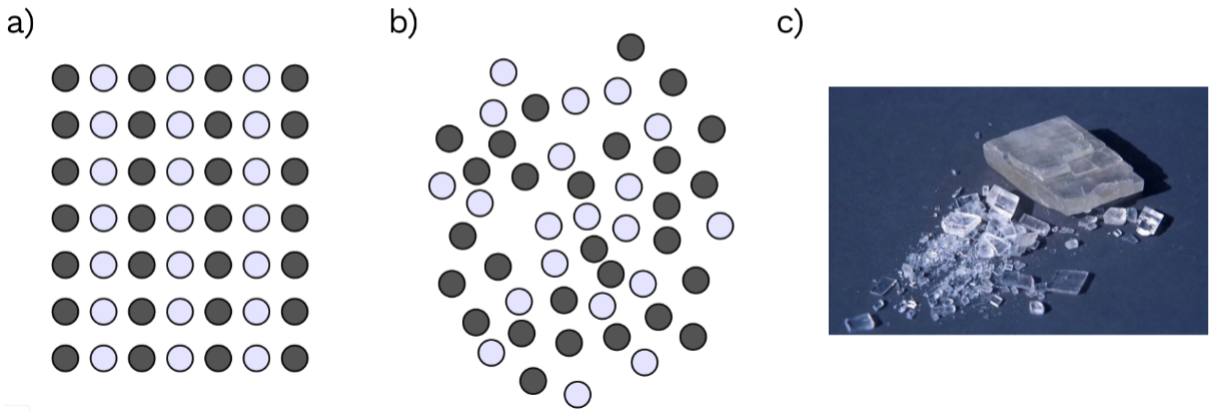

Figure 2.5. a) Structure of a plane diatomic crystal. Notice that it is not isotropic, but it has a high level of homogeneity. b) Amorphous material. Look at how randomly the particles are placed. c) Cleavage of a crystal along its crystalline planes. Image taken from [39].

The main significance of crystalline solids hovers over the presence of well-defined properties that go from sharp melting points to characteristic cleaving planes, and as a matter of fact, especially due to their homogeneity, we are always in a safe spot to say what the material is like, and how it behaves under any circumstances, which is a must when the material itself is not the main focus of our study. In short, one should keep in mind the following points regarding crystalline and amorphous solids [52]:

Crystalline:

- Characteristic geometrical shape;

[2] It has the same stuff everywhere.

- Long order arrangement, which indicates a well-defined melting point;
- Anisotropic[3] by nature;
- One can smoothly cut them along specific planes;
  - Sodium Chloride, Diamond, Germanium, Samarium Hexaboride;

Amorphous:

- No definite geometrical shape;
- Melting processes take place over a temperature range;
- Isotropic by nature;
- Don't break at fixed cleaving planes;
  - Glass, plastics, ceramic;

One can still classify crystalline solids according to their interatomic bonds in ionic, molecular, covalent, and metallic. Finally, all that concerns crystals can be understood with the help of the following diagram:

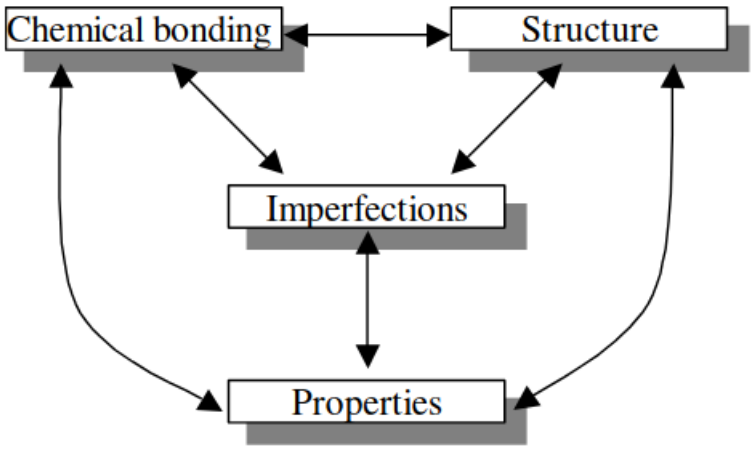

Figure 2.6. Source points of all crystals' properties and their relationships. Image taken from [52].

[3]The property being measured depends on the direction along which they are measured.

Now we know what crystals look like as well as their main properties, it is time to delve into the subsequent question of how we study them. That leads us to the concept of lattices, and especially Bravais lattices, which are carefully discussed next.

2.2.2 Bravais Lattices

By standard, our first step in studying any objects or systems in Physics consists of setting up a coordinate system that enables us to represent the entire system and its time evolution. For clarity's sake, it is shown below a diatomic crystal and a possible coordinate system:

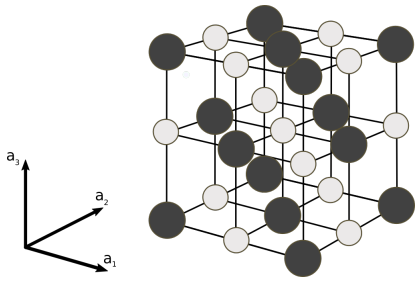

Figure 2.7. Diatomic crystal.

Moreover, when we delve into this crystal study, we promptly notice its translational symmetry, which can be highly exploited by choosing a collection of atoms that stands for a minimal set whose reproduction spans the whole crystal in all directions. In doing so, we will have changed our description to a Bravais lattice plus a base as follows:

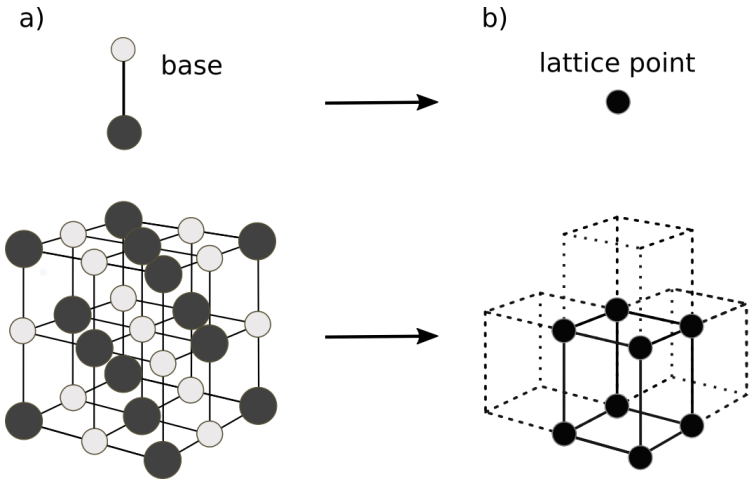

Figure 2.8. a) Crystalline solid and a possible base for its representation. b) Bravais lattice related to the crystal shown in (a).

We can still make it more general and say that "Every crystal can be depicted by a Bravais lattice with a base.", where a Bravais lattice, also known as direct lattice, is just an infinity set of homogeneous, and isotropic points[4] such as the ones depicted on the right in figure 2.8. Finally, it is important to note that if we plug our base into all the Bravais sites[5], we will simply end up with our crystal again. In other words, we have only shown a way to depict crystals in general exploiting their translation symmetry a little further.

In what concerns a Bravais lattice, its high homogeneity, and especially its isotropy, assure us to find the same properties everywhere, which leads us to the concept of cells, the most important one in crystallography. This structure consists of a collection of sites, such as the emphasized cube on the right-hand side in figure 2.8, whose reproduction spans the entire lattice. Besides, we may also take different cells depending on our purposes[6], being the primitive cell the most important one. This one encloses the smallest volume possible and only encompasses one lattice site, for example, the one in figure 2.8 looks like it has 8 sites, but once *they are being cut* by the lattice, the cell itself only has $8 * 1/8$ sites at the end, that is, 1 site. Finally, their nomenclature is based on their distinctive geometric characteristics. The main types are listed next [5]:

- Simple Cubic (SC): This cell type represents the most basic arrangement, where the lattice points are located at the corners of a cube, and there is one lattice point per unit cell;

- Face-Centered Cubic (FCC): In an FCC cell, the lattice points are situated not only at the corners of the cube, but also at the centers of each of the cube's faces, resulting in a total of four lattice points per unit cell;

- Body-Centered Cubic (BCC): The BCC cell features lattice points at the corners of the cube, just like the SC cell, but it also has one additional lattice point at the center of the cube, totaling two lattice points within each unit cell;

- Closed-Packed Hexagonal: This cell type is characterized by a hexagonal arrangement of lattice points in two layers, with the third layer placed directly above the first, resulting in a densely packed structure with multiple lattice points per unit cell;

[4] Notice, though, that these points do not have a standard nature. They can be whatever you set for the base.
[5] A site is one point of the lattice.
[6] We have the following types of cells in crystallography: primitive, unitary, and supercell.

- Simple Hexagonal (SH): The lattice points form a hexagonal arrangement with one lattice point per unit cell, and it does not involve the stacking of multiple layers;

Lastly, before diving into other questions no longer directly related to cells, such as symmetry and band structures, it is worth giving some special attention to Fourier transforms and their physical meaning in material science. Let's approach the question by considering a plane wave that has the same periodicity as the Bravais lattice under study. Since all sites of our lattice are described by:

$$\mathbf{R} = n_1\mathbf{a}_1 + n_2\mathbf{a}_2 + n_3\mathbf{a}_3 \tag{2.8}$$

where $\mathbf{a}_1$, $\mathbf{a}_2$, and $\mathbf{a}_3$ are any three vectors, not all in the same plane, and n_1, n_2, and n_3 are integers[7], and recalling that a moving forward plane wave is given by:

$$\psi(\mathbf{r}, t) = \sin(\mathbf{k}\cdot\mathbf{r} - \omega t) = \mathrm{e}^{i(\mathbf{k}\cdot\mathbf{r}-\omega t)} \tag{2.9}$$

in what follows, we can fully encompass the assumption by equalling the latter expression at two different points displaced by $\mathbf{R}$, which is simply:

$$\begin{aligned} \psi(\mathbf{r}, t) = \psi(\mathbf{r}+\mathbf{R}, t) \quad \Longrightarrow \quad \mathrm{e}^{i(\mathbf{k}\mathbf{r}-\omega t)} &= \mathrm{e}^{i[\mathbf{k}\cdot(\mathbf{r}+\mathbf{R})-\omega t]} \\ \mathrm{e}^{i\mathbf{k}\mathbf{r}}\mathrm{e}^{-i\omega t} &= \mathrm{e}^{i(\mathbf{k}\cdot\mathbf{r}+\mathbf{k}\cdot\mathbf{R}-\omega t)} \\ \cancel{\mathrm{e}^{i\mathbf{k}\cdot\mathbf{r}}}\cancel{\mathrm{e}^{-i\omega t}} &= \cancel{\mathrm{e}^{i\mathbf{k}\cdot\mathbf{r}}}\mathrm{e}^{i\mathbf{k}\cdot\mathbf{R}}\cancel{\mathrm{e}^{-i\omega t}} \\ 1 &= \mathrm{e}^{i\mathbf{k}\cdot\mathbf{R}} \end{aligned} \tag{2.10}$$

and thus:

$$1 = \mathrm{e}^{i(\mathbf{k}\cdot\mathbf{R})} \iff 1 = \cos\mathbf{k}\cdot\mathbf{R} + i\sin\mathbf{k}\cdot\mathbf{R} \quad \Longrightarrow \quad \mathbf{k}\cdot\mathbf{R} = 2\pi\mathrm{m} \quad , \quad \text{where } \mathrm{m} \in \mathbb{Z} \tag{2.11}$$

Now let's analyze one of the possible three directions, let's say, $\mathbf{a}_1$. In this case, if we recall that

[7] The point $\mathbf{R}$ is reached by moving n_i steps in the $\mathbf{a}_i$ direction for $i = 1$, 2, and 3.

$\mathbf{b}_i \cdot \mathbf{a}_j = 2\pi\delta_{ij}$, the expression above becomes:

$$\begin{aligned}\mathbf{k}\cdot\mathbf{R} \iff (k_1\mathbf{b}_1 + k_2\mathbf{b}_2 + k_3\mathbf{b}_3)\cdot(n_1\mathbf{a}_1) &= k_1n_1\mathbf{b}_1\cdot\mathbf{a}_1 + k_2n_1\mathbf{b}_2\cdot\mathbf{a}_1 + k_3n_1\mathbf{b}_3\cdot\mathbf{a}_1 \\ &= k_1n_1 2\pi\delta_{11} + k_2n_1 2\pi\cancel{\delta_{21}} + k_3n_1 2\pi\cancel{\delta_{31}} \\ &= k_1n_1 2\pi\end{aligned} \tag{2.12}$$

where we used the following general properties of Kronecker deltas:

$$\begin{cases}\delta_{ii} = 1 \\ \delta_{ij} = 0 \Leftrightarrow i \neq j\end{cases} \implies \quad \delta_{11} = 1\ ,\ \delta_{21} = 0\ ,\ \delta_{31} = 0 \tag{2.13}$$

Lastly, since $\mathbf{k}\cdot\mathbf{R} = 2\mathrm{m}\pi$, we find:

$$k_1n_1\cancel{2\pi} = m\cancel{2\pi} \implies k_1n_1 = m \tag{2.14}$$

The same reasoning may be followed for the other two directions, which prompts us to two different and important conclusions. First, the consideration of plane waves led us initially to equation 2.11, which is precisely a discretization of k-space, also known as momentum space. Afterward, by picking up a specific direction, we reached 2.14, which by its turn indicates that besides being discrete, all k are also integers, after all, m is an integer. In short, when we supposed plane waves with the same periodicity of the lattice, which was simply taking its Fourier transform, we got another space directly related to our Bravais lattice, which was also a Bravais lattice [5]. For these reasons, as long as we are dealing with a Bravais Lattice, this one, directly related to it, is called reciprocal lattice.

It is worth noting that a good understanding of what is the momentum space and how it is related to the direct lattice is necessary as far as our band structures are gotten within the former. At last, in the same way as we did before for the direct lattice by setting up some cells to describe it, we also do it for the reciprocal lattice. Here, however, the most important lattice cell is no longer called primitive cell, although it is still a primitive one, but Wigner-Seitz cell instead. This construct is not only the primitive cell of the reciprocal lattice, but also gathers all the symmetries of the lattice, being used on the band structure generation. In the next section, before diving

into band structures, we are going to give some special attention to what are symmetries, how we identify objects of symmetry and their role in material science.

Keywords about Lattice Structures

As long as we are handling crystals, we usually find two well-known terms that are worth our attention. The first one is called bulk, which stands for a region within the crystal that is out of any interference from both the region outside the material and surface effects, while the other is called lattice parameter. The latter represents the distance between two adjacent lattice sites and is usually described by non-capitalized letters, such as a, and k, as used previously. Lastly, they are obtained experimentally using X-ray diffraction, and to understand that, all we have to do is to recall that waves are scattered in all directions whenever they find an obstacle that has dimensions of the order of its wavelength[8], interfering with itself afterward. Such interference may be constructive or not in such a way that if we place a moving target around the material, we will inevitably notice regions of light and dark side-by-side. There are two main laws concerning X-ray diffraction in solids, they are Bragg's and Laue's. Note, though, that they are just different developments of the same physics. In the figure below, we present the main assumptions of Bragg's law and how it can be used to predict the lattice parameter of a crystal [5]:

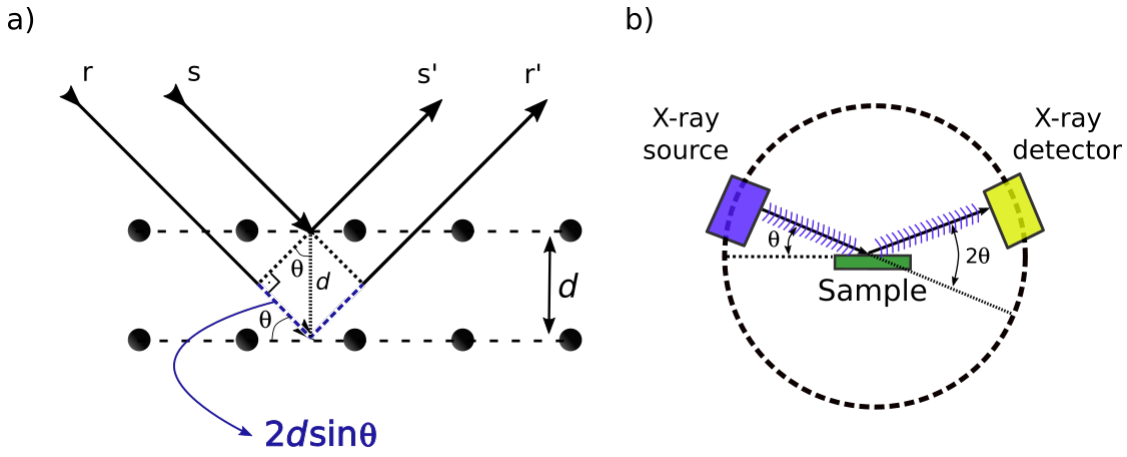

Figure 2.9. a) Two parallel incident X-ray beams, **r** and **s**, are scattered on adjacent lattice planes, resulting in two parallel beams **r'** and **s'**. b) A possible device using X-ray diffraction to measure lattice parameters. Image taken from [22].

[8] X-rays are used here because lattice parameters are usually of the order of 10^{-9} m, which is within the X-ray wavelength range in the electromagnetic spectrum.

Recalling that for waves to interfere destructively one's crests must overlap the other's troughs[9], and considering the two beams being initially in phase, we can promptly conclude from the image that, in order to interfere constructively, the length the left-most beam went farther than the other must be equal to an integer number of wavelengths. In other words:

$$2d \sin\theta = n\lambda \tag{2.15}$$

where $n \in \mathbb{N}$, and λ is the source's wavelength. Finally, once all crystal parameters were obtained, we set a computer to slightly vary the position of all atoms within a cell to ensure we are working with the most stable structure from a theoretical point of view. In this approach, it is searched for the configuration where the net force on all atoms is under a beforehand set value, and the system's energy is a global minimum[10]. This procedure is called relaxation process[11], and sometimes it is really tricky to point out whether we found a local or a global minimum for the energy, the former being the source of future errors[12].

To understand what are band structures and how they are gotten in material science, we are going to skim over group theory and its main implications in the following subsection.

2.2.3 Symmetries

When we first start studying regular materials like the ones found in material science, the most remarkable properties are given by their regularity in what concerns rotations, reflections, and displacements. Furthermore, by the time we dive into their structures to reach a higher level of understanding, we may also notice that the whole operation may be broken down into two different elements, the operation itself, which is the action of doing something, and the object upon which it is being done. Finally, note that the name symmetry is used to specify operations that leave the object unchanged at the end of the process exactly as in figure 2.10 [56].

[9] Crests and troughs are the highest and lowest points of plane waves, respectively.
[10] These two constraints fully encompass all requirements for a stable configuration.
[11] By standard, it is our first step whenever we start analyzing a new material.
[12] A further discussion is found in [21].

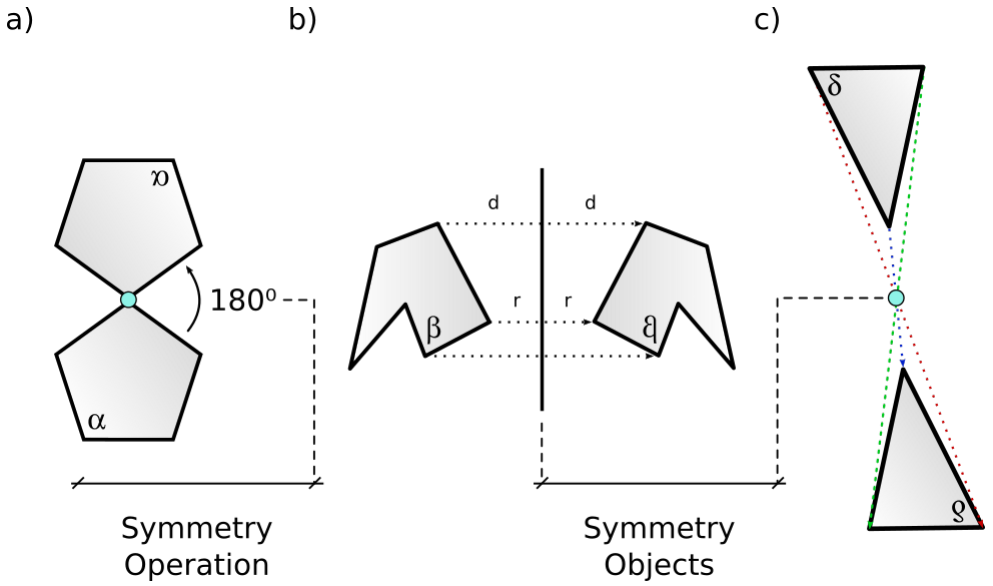

Figure 2.10. Three of all five symmetry operations. a) Rotation. b) Reflection through a plane. c) Reflection through a point.

Here, it was depicted three out of the five symmetry operations to explicitly outline to the reader what should be kept in mind as long as we are talking about symmetries and symmetry objects. Note still that in the material science field, all symmetry objects are denoted by Greek letters as in the following figure:

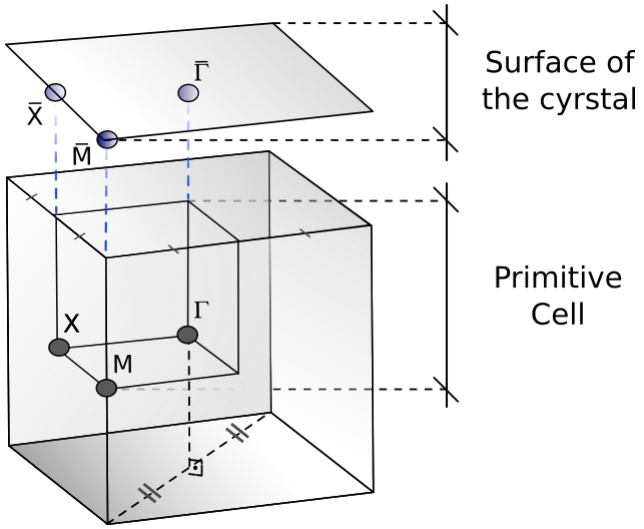

Figure 2.11. Primitive cell (smaller cube) and its high symmetry points.

Regarding the superscript line over some letters, they are used to emphasize we were dealing with

the surface of the material instead of its bulk[13].

Lastly, besides being used to classify materials in groups according to their internal symmetries, they may also be understood as a natural constraint that is being applied to the final wave function of all particles. As an example, since all crystals must have a translational symmetry, Bloch carefully analyzed its consequences for all electrons' wave functions finding that we not only had $\psi(\mathbf{r})$, but:

$$\psi_{n\mathbf{k}}(\mathbf{r}) = e^{i\mathbf{k}\cdot\mathbf{r}} u_{n\mathbf{k}}(\mathbf{r}) \tag{2.16}$$

or simply

$$\psi(\mathbf{r}+\mathbf{R}) = e^{i\mathbf{k}\cdot\mathbf{R}}\psi(\mathbf{r}) \tag{2.17}$$

where u is a periodic function that only depends on the material under study [5]. Before jumping to band structures, which stand for the heart of material science, it is worth noting that all symmetries are studied in the reciprocal lattice, but since the direct and reciprocal spaces are connected through Fourier transforms, which are linear, we can safely analyze them within the real space.

2.2.4 Band Structures

This subsection is going to be developed in three steps, what are band structures, why we study them, and what they look like. The first point is promptly derived from the following assumption: as long as we are dealing with quantum-bonded systems, such as molecules and crystals, we can safely say that their energy levels are going to be discrete. To fully understand it, we can come up first with a free particle whose wave function and energies will respectively be given by:

$$\psi(\mathbf{r}) = e^{i\mathbf{k}\cdot\mathbf{r}} \qquad , \qquad E_k = \frac{\hbar^2 k^2}{2m_e} \tag{2.18}$$

Then, if we simply add a conservative potential, such as an electric one, to the system, its wave functions will no longer be given by plane, and their energies will become discrete. A simple example of this phenomenon is observed in hydrogen-like systems such as all alkaline metals whose spectra are quite similar to the one shown in figure 2.12 [5, 17]. In what follows, a good way to

[13] Bulk is a region of the material that is out of any borders' effects.

better understand what band structures are may be reached by addressing the following question: what happens when we bring two atoms together? What if we place a bunch of them side by side like in a crystal? First, since we are dealing with Fermionic particles, they must obey Pauli's exclusion principle[14], plus the electric field of each atom will inevitably affect the other one's particles. Consequently, since each orbital has a specific configuration and storage, plus the fact the electric potential depends on these variables, the energy spectra of two atoms will look like the one of a single atom despite the fact its levels will come from the latter by an unfolding process. Finally, if we place more atoms together, more orbitals will be unfolded. Another qualitative and halfway understanding of this process is given by the following assumption: all orbitals are slightly unfolded to satisfy Pauli's exclusion principle, otherwise we would end up having many electrons in the same region with the same states. Therefrom, if we apply this reasoning to a crystal, we promptly notice its orbitals' energies will look like an almost continuous spectrum, even though each "block", also known as a band, will be composed of discrete states. The idea here outlined through words is depicted in picture 2.12 for all three cases, a single, two, and a bunch of atoms regularly displaced.

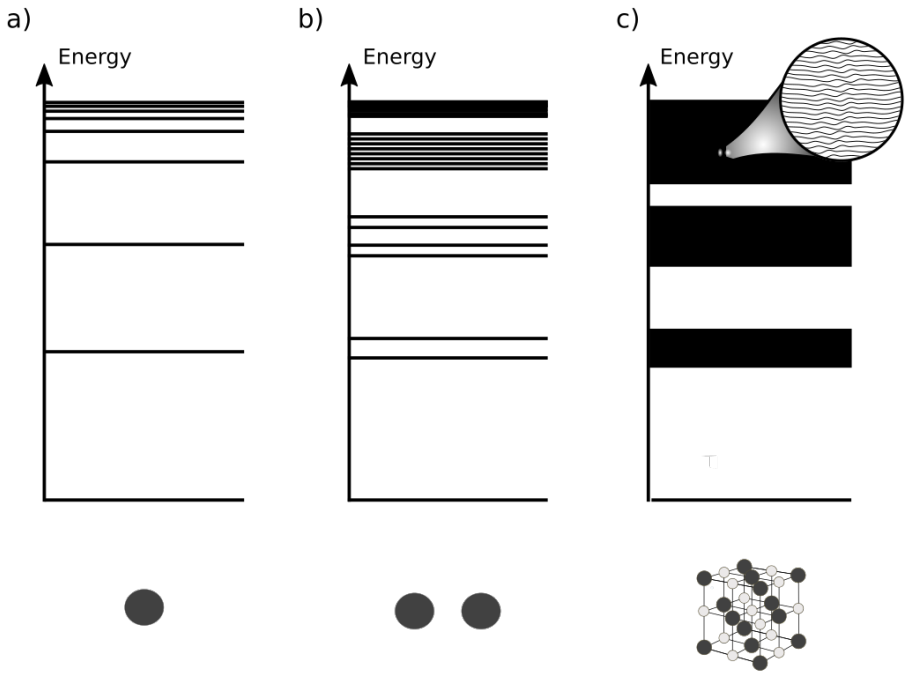

Figure 2.12. Energy spectrum of a single (a), two (b), and a bunch of atoms (c) displaced regularly in space.

[14] This terminology will be further discussed in the next subsection.

In what concerns crystals, we can still make good use of these band structures and manage to find out all properties of the materials as will be further explained in the next sections and chapters. Besides, since we can't lose sight of Pauli's exclusion principle, those bands are always filled bottom-up the same way as in lonely atoms. There may also be a space, also known as a *gap*, between each band, and if some of those bands are completely filled, then as long as the provided energy is less than the gap energy, all electrons will have nowhere to go and the whole material will behave as an insulator. On the other hand, if we make the gap smaller so its energy is of the order of the environment's thermal energy, then the most energetic electrons will make it to the upper band giving some "movement" to the material which will take the object to a fairly conducting set of materials, also known as semiconductors. For clarity's sake, take a look at figure 2.13.

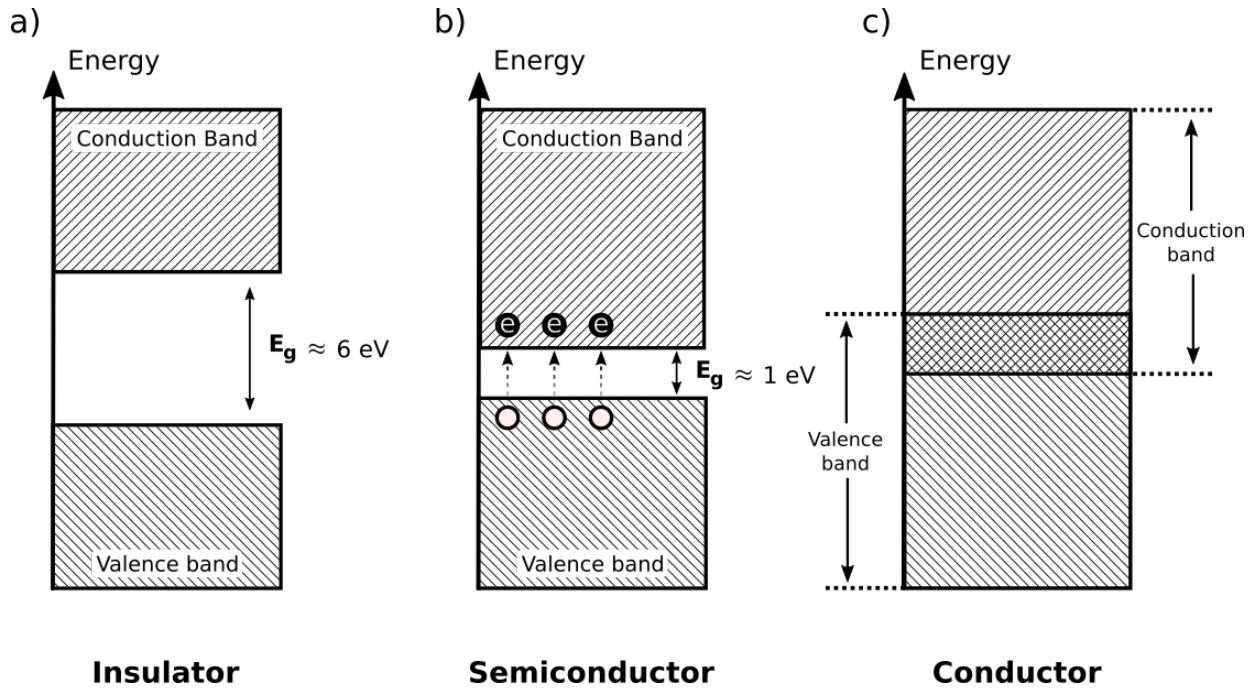

Figure 2.13. Classification of all materials according to their band structures in what concerns transport properties.

Finally, note that conductors have a continuous-like band structure that allows their electrons to move freely through all states within the material [5].

In practical terms, it is interesting to note that all the states of these electrons are studied in k-space where each point (k_x, k_y, k_z) is associated with a set of eigenstates, each one having its own energy. So if we cut a plane out in k-space, we will find a 2D energy distribution like the one

in figure 2.14.

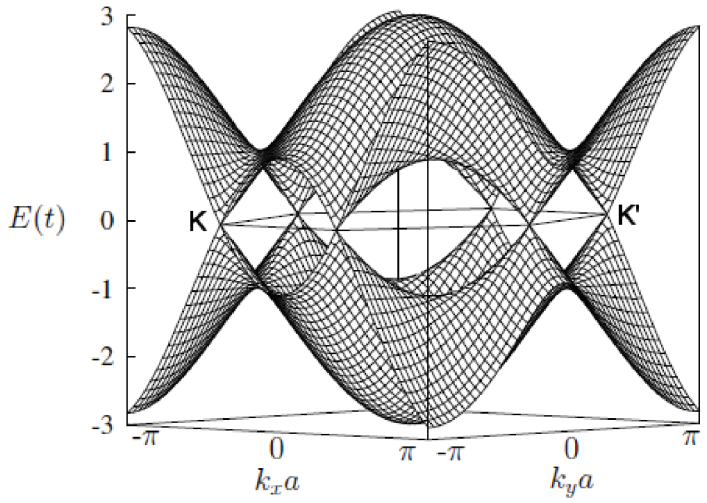

Figure 2.14. a) Graphene band structure for a fixed k_z. Image taken from [42].

In what follows, we are going to skim over the last two topics concerning the necessary overview before jumping to the numeric method and the results, they are Fermi energy and topology.

2.2.5 Fermi-Dirac Distribution

Even though we can distinguish atoms according to their electrons and nuclei, we can make no difference between either two electrons or two protons. They look the same in all ways, ever, which means that if we interchange their positions, the wave function of the system must remain unchanged. In other words, if we are considering two independent electrons, we could come up first with the following total wave function:

$$\Psi(1,2) = \psi_1(\mathbf{r}_1)\psi_2(\mathbf{r}_2) \tag{2.19}$$

but it would be just physically unacceptable because it does distinguish between the particles, which may be noticed by interchanging their positions through $\Psi(1,2) = \Psi(2,1)$. Consequently,

Ψ must be either symmetric or anti-symmetric, which is simply:

$$\begin{aligned} C(\psi_1(\mathbf{r}_1)\psi_2(\mathbf{r}_2) + \psi_1(\mathbf{r}_2)\psi_2(\mathbf{r}_1)) &\implies \Psi \text{ is symmetric} \\ C(\psi_1(\mathbf{r}_1)\psi_2(\mathbf{r}_2) - \psi_1(\mathbf{r}_2)\psi_2(\mathbf{r}_1)) &\implies \Psi \text{ is anti-symmetric} \end{aligned} \tag{2.20}$$

where C is just a normalization constant. These functions establish the base of two different distributions broadly known as Bose-Einstein (symmetric) and Fermi-Dirac (anti-symmetric). Particles that obey the Bose-einstein distribution, simply called bosons, manage long-range interactions between particles and have an integer spin. For instance, in what concerns bosons, we could talk about gravitons and photons, which manage gravitational and electromagnetic interactions, respectively. Fermi-Dirac particles, on the other hand, or simply fermions, stand for one kind of particle whose spin is a half-odd-integer. For example, in this case, we could think of electrons and protons. Finally, note that while making $\Psi(1,2) = \Psi(2,1)$ for bosons doesn't turn out to be an issue, doing that for fermions leads us to the following remarkable result:

$$\Psi(1,1) = C(\psi_1(\mathbf{r}_1)\psi_2(\mathbf{r}_1) - \psi_1(\mathbf{r}_1)\psi_2(\mathbf{r}_1)) = 0 \tag{2.21}$$

The aforementioned consequence of fermions' antisymmetry is called Pauli's exclusion principle and hovers over all interactions among fermions such as electrons and protons. One of its immediate corollaries is that whenever we have a bunch of electrons within the same region in space, their energies can't be the same, so if we are filling up some available states with electrons, we must always start with the lowest available level, and *put* the next electron one level higher than the last one. For instance, if we bring together a bunch of independent and free electrons, they will occupy all states continuously up to the limit state e_f, which is called Fermi level. In its turn, due to its remarkability, all properties related to this state, such as the one we are interested in here, fermi velocity, carry the name Fermi along [5, 48]. It is worth noting, though, that we have only considered free independent electrons at $0\,\mathrm{K}$ so far, and adding some temperature or other greatnesses to the system will inevitably affect the energy distribution of all electrons as depicted in figure 2.15.

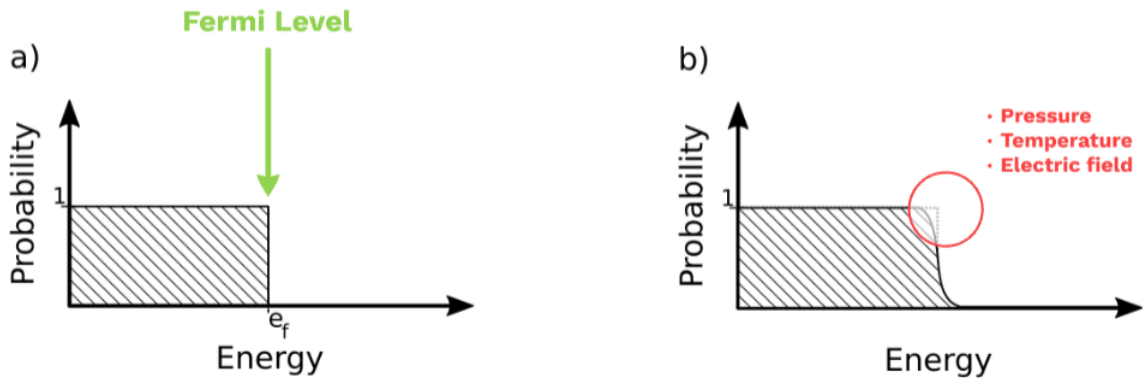

Figure 2.15. a) If we place a bunch of free and independent electrons together, they will occupy all adjacent levels continuously up to the fermi level. Consequently, the probability of finding an electron at any level before the fermi level must be equal to 1. b) When we add other greatnesses to the system, such as temperature or pressure, they will initially affect the most energetic levels reshaping their distribution [48].

So far, despite considering free and independent elections, we haven't considered the vectorial nature of **k** yet. Doing so, we promptly find that those planes become a sphere due to the following proportion:

$$Energy \propto \mathbf{k}^2 = (k_x^2 + k_y^2 + k_z^2) = r_f^2$$

where r_f is known as the Fermi radius[15].

In what follows, since it is a fundamental part of the current work, we are going to develop a way to find some materials' Fermi velocity from their band structures.

Fermi velocity

First, it is worth noting that the Fermi velocity is a greatness directly related to the Fermi level and as far as we are handling a quantum particle, we can connect its crystalline momentum to the classical definition of momentum in a semi-classical approach. This will deliver us an equality for **v** as follows:

$$\hbar\mathbf{k} = m^*\mathbf{v}_f \Longrightarrow \mathbf{v}_f = \frac{\hbar\mathbf{k}}{m^*} \tag{2.22}$$

where m^* is the effective mass of the electron [4]. It is worth noting that despite being a mass, m^* is not equal to the real mass of the electron. It is just a numerical constant that enables us to connect the classical and the quantum worlds through their momentums. Then, from this

[15] Further information may be found in [48].

point on, we are mainly interested in addressing the following question: how do we find it? One possible approach that fits incredibly well in all development we have made so far is given by the connection between three main concepts found in classical and quantum mechanics: De Broglie's postulate, group velocity, and Newton's second law. Starting with the first two, we get:

$$\begin{cases} E = \hbar\omega \\ v_g = \dfrac{\partial\omega}{\partial k} \end{cases} \implies \frac{\partial E}{\partial k} = \hbar\frac{\partial\omega}{\partial k} = \hbar v_g \implies \frac{\partial}{\partial t}\frac{\partial E}{\partial k} = \hbar\frac{\partial v_g}{\partial t} \tag{2.23}$$

Then, since E is differentiable and is both a function of k and t, we can safely employ the chain rule and rearrange it as:

$$\frac{\partial}{\partial t}\frac{\partial E}{\partial k} \equiv \frac{\partial}{\partial k}\frac{\partial E}{\partial t} \equiv \frac{\partial}{\partial k}\frac{\partial E}{\partial k}\frac{\partial k}{\partial t} \equiv \frac{\partial^2 E}{\partial k^2}\frac{\partial k}{\partial t} \tag{2.24}$$

we may then plug it into 2.23 plus the well-known result $\dot{v} = a$ to find:

$$\frac{\partial^2 E}{\partial k^2}\frac{\partial k}{\partial t} = \hbar a \tag{2.25}$$

where **a** is simply the total acceleration of the electron. On the other hand, employing Newton's second law, we find:

$$F = \frac{\mathrm{d}}{\mathrm{d}t}(mv) \implies F = \frac{\partial}{\partial t}(\hbar k) = m^* a \Rightarrow \frac{\partial k}{\partial t} = \frac{m^* a}{\hbar} \tag{2.26}$$

We may then plug 2.26 into 2.25 to find:

$$\frac{\partial^2 E}{\partial k^2}\frac{\partial k}{\partial t} = \hbar a \implies \frac{\partial^2 E}{\partial k^2}\frac{m^* a}{\hbar} = \hbar a \Rightarrow m^* = \frac{\hbar^2}{\frac{\partial^2 E}{\partial k^2}} \tag{2.27}$$

Finally, note that the first derivative, namely

$$\frac{\partial E}{\partial k} = \hbar v_g$$

didn't mention the chosen direction at any moment while we do have $\mathbf{k}_x$, $\mathbf{k}_y$, and $\mathbf{k}_z$ in k-space. Consequently, if E at a specific point (k_x, k_y) changes accordingly to the direction we move, then

the aforementioned development would have led us to the following tensor instead:

$$m^* = \frac{\hbar^2}{\frac{\partial^2 E}{\partial k_\alpha \partial k_\beta}} \tag{2.28}$$

where α and β stand for a direction in k-space exactly as we had for the directional derivative. As an example, to analyze whether we should consider directions or not, we could cut out the Fermi level from the band structure and take a closer look at the k-point where the optical transition is taking place. For instance, let's say that figure 2.16 stands for the last band of a hypothetical semiconductor, namely, its Fermi level. Then, if we take a closer look at one of its most energetic points as in figure 2.17, we will note that no matter what direction we move along, we will inevitably find the same thing all the time. Then, due to this symmetry, we can safely use the former development instead of the latter to find its effective mass.

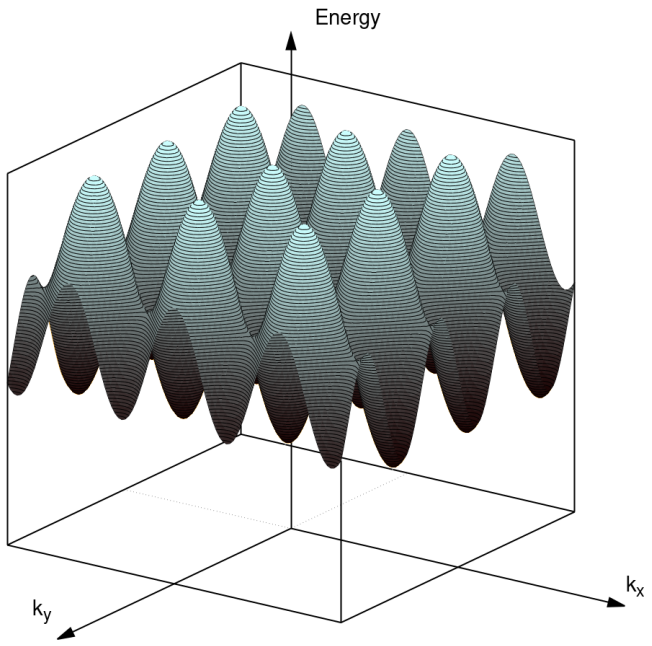

Figure 2.16. Pictorial valence band of a semiconductor.

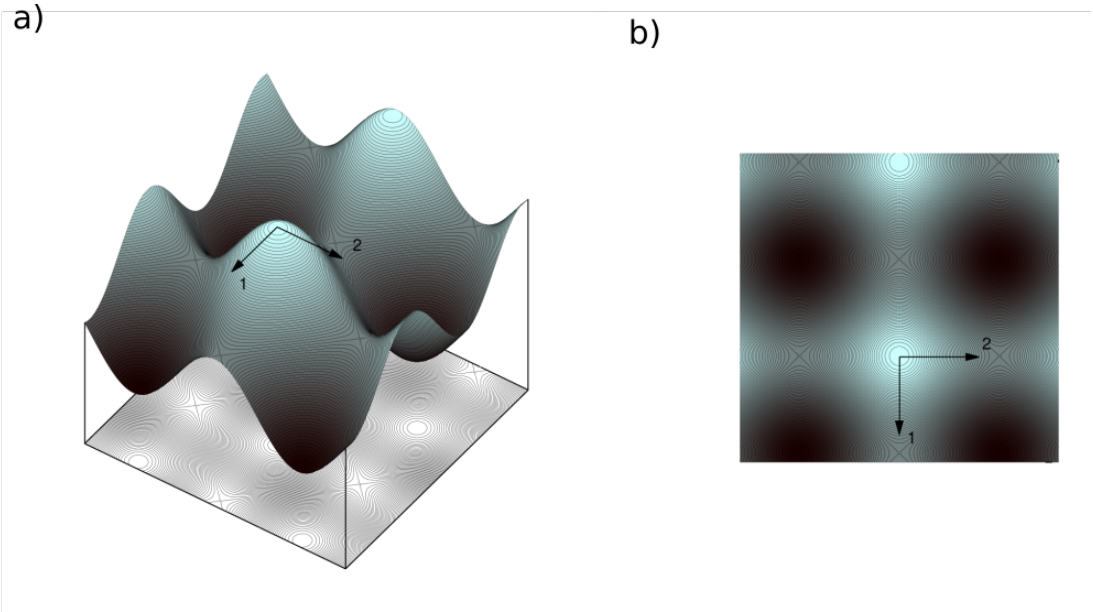

Figure 2.17. a) Cut of a region. b) Top view of the point where an optical transition may take place.

2.2.6 Topology

Throughout the past century, it was believed that materials could only have their phase changed by a spontaneous symmetry break. Despite that, it was discovered that some crystals could remarkably have their properties changed continuously. For instance, SmB_6 is naturally a semiconductor, but as temperature goes down, its bulk becomes an insulator while its surface reaches a metallic *plateau*, as will be further explored [34]. In such a case, the final object seems no longer connected to the former due to its highly different conducting properties. Moreover, differently from Ehrenfest's classification [27], we can't find an order parameter that goes to zero in the trivial phase and assumes a non-zero value in the non-trivial phase.

Topological materials may be classified in a similar way to the one found in math topology. There, if two materials have the same number of holes, called genus numbers, then each can be continuously reshaped up to the limit where they both have the same form. If that is true, then we say they have the same topology. In material science, though, we are remodeling their Hamiltonian through adiabatic transforms instead. The whole idea here exposed is depicted in figure 2.18.

In short, topological insulators are materials whose bulk behaves as an insulator, while their

surfaces have temporal symmetry-protected states that give the material a well-localized metallic nature. In what concerns their band structures, we find the semiconductor-like distribution as expected for the bulk and a linear distribution shaped as a Dirac cone for surface states [2].

Lastly, regarding trivial systems, these are the ones whose Hamiltonian can be continuously reshaped up to the atomic level without any abrupt changes in the material's properties, such as a gap closing. At the end of the process, we would no longer have a superposition of states as if we were handling a set of discrete atoms and our solutions would now concern this system. On the other hand, if that doesn't turn out to be true, then the object is called topological [7]. To predict them theoretically, we first search for a band inversion between valence and conduction bands, where the orbitals found in one band abruptly change to the other band, and inversely, as will be shown in the results. Afterward, we find either, its topological invariant, or its surface-protected states. At this point, we will be in a safe spot to say whether we are working with a material that has a trivial or non-trivial topology.

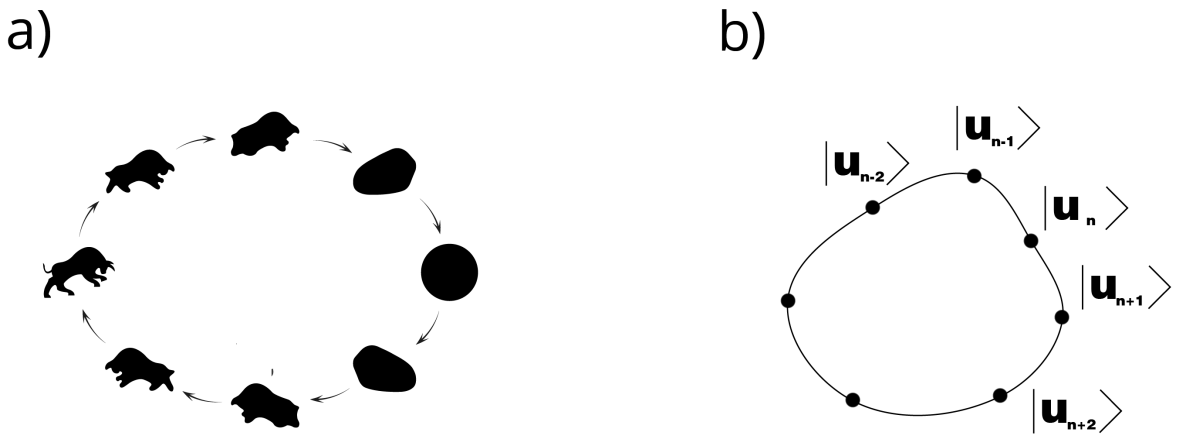

Figure 2.18. a) The cyclic process of reshaping an ox up to the limit where it becomes a sphere. b) Analogous cyclic process of reshaping a Hamiltonian operator through adiabatic transformations.

2.3 Hexaborides

First, regarding hexaborides in general, it is worth noting that the cubic structure shown in 2.19 is shared by all compounds of the form XB_6, in which a metallic atom is surrounded by 24 boron atoms in octahedral arrangements.

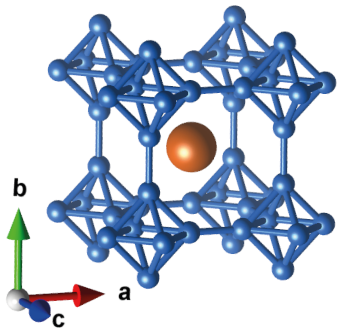

Figure 2.19. Metallic atom encapsulated by boron atoms in a XB_6 structure.

It is also noteworthy that microscopic particles of these materials often assume a cubic shape as a mirroring of the crystalline structure. Additionally, the coordination number of Boron is 5, while that of the element X is 24, something that can be immediately visualized through graphic software. Thus, the valence electrons of boron emerge from 5 bonds, and it should be noted that the material itself would not exist if electrons from the metallic element were not donated to the crystalline structure. Besides, chemical bonds between boron atoms in a hexaboride are strong enough to impart high hardness and a high melting point to the material. Besides, there is a large range in their electronic conductivity that forms the core of their applications in optoelectronics. It is also noteworthy that this property can be adjusted through the modification of the atom trapped within the boron network. To stabilize within the network, though, this element must release either two or three electrons to the boron atoms, and that's where the play begins [10].

It has been experimentally and theoretically observed that when the central atom donates two electrons to the network, these divalent hexaborides exhibit a semiconductor character, in contrast, trivalent hexaborides possess a metallic character[16]. It is also noteworthy that dangling bonds and impurities, even in the smallest proportions, can cause divalent compounds to exhibit metallic characteristics. These observations lead us to the idea that we do not have complete freedom to choose the metallic atom to be encapsulated by the boron cage, as it must have at least a double valence[17] and cannot be excessively large. After all, the interactions between boron atoms are intense and give rise to a closed structure for them. Therefore, it can be concluded

[16] This variation in material conductivity has been explained through gap overlaps and carrier concentration.
[17] The compound KB_6 has already been produced in a controlled environment.

that this atom must necessarily belong to one of the following groups: alkali-earth metals, rare metals, or some actinide metals [10].

Lastly, it is presented in table 2.1 some crystallographic data for selected borides. This data confirms that the lattice parameters do not vary much from one substance to another, indicating that the main agent in structuring the material is the Boron. Then, the overall stability of the structure only depends on two factors: the vapor pressure of the metallic cation and the stability of the bonds between boron atoms [8, 10].

MB_6	a (Å)	B-B_{in} (Å)	B-B_{out} (Å)
KB_6	4.2246	1.8033	1.6744
CaB_6	4.1514	1.7520	1.6760
SrB_6	4.1953	1.7620	1.7040
YB_6	4.1000	1.7460	1.6300
BaB_6	4.2618	1.7800	1.7440
LaB_6	4.1569	1.7660	1.6590
CeB_6	4.1407	1.7511	1.6644
NdB_6	4.1269	1.7574	1.6415
SmB_6	4.1346	1.7438	1.6688
EuB_6	4.1849	1.7596	1.6964
YbB_6	4.1479	1.7525	1.6695
ThB_6	4.0931	1.7570	1.6100

Table 2.1. Crystallographic data for selected borides. Table taken from [10].

2.3.1 Samarium Hexaboride (SmB_6)

Despite being widely studied, the mixed-valence material SmB_6 turned out to be challenging for theoretical study, especially due to its highly localized f-states, besides its high density of d and f states in the valence band. Regarding its study, it is still noteworthy that the possibility of SmB_6 being a topological Kondo insulator has recently rekindled interest in the material, and several follow-up experiments have been actively conducted to confirm this theory (KANG *et al.*, 2015b). Lastly, even though its topological nature could be pointed out by the existence of in-gap states with a Dirac-cone dispersion, its narrow band gap, and half-flat valence band make it difficult to observe in-gap states near the Fermi level [29].

Production

Even though we find a wide range in hexaboride properties, by standard, our first step into studying any new material must be searching for whether it may produced or not. At this point, it is important to keep in mind that the melting point of SmB_6 is pretty high (about 2400 ºC) [34]. Consequently, since it is higher than the melting point of Aluminum, it can be grown employing the flux method, where polycrystalline powders of SmB_6 are dissolved into an aluminum flux at lower temperatures ($\approx 1,450$ ºC) and then cooled down while the naturally generated temperature gradient crystallizes SmB_6 [34]. This polycrystalline, on the other hand, can be produced through molten salt electrolysis where the following total reaction

$$2\ Sm_2O_3 + 12\ B_2O_3 \longrightarrow 4\ SmB_6 + 22\ O_2 \tag{2.29}$$

takes place and the dissociated Sm and B ions adhere to a molybdenum (Mo) cathode forming the compound SmB_6[18], which will be then deposited at the bottom of the system [8]. Figure 2.20 illustrates the general idea of this procedure, while the images presented in 2.21 outline what this powder may look like at the end of the electrosynthesis process.

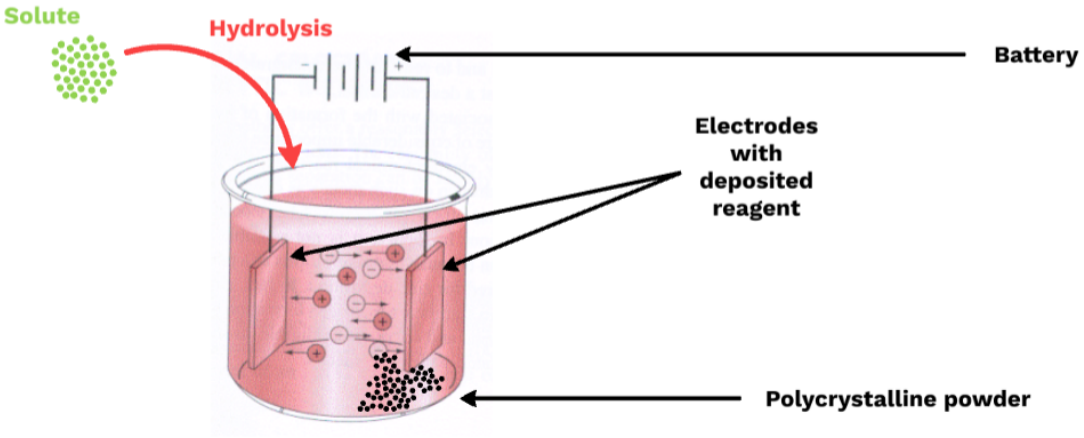

Figure 2.20. Electrosynthesis of a polycrystalline powder. A compound is dissolved into water and broken down into smaller charged particles, called ions. These, due to the electric field generated by the battery in the solution, move towards the plate oppositely charged and react with the deposited reagent, releasing or taking some electrons in the process and ending up neutralized. In the end, this neutralized compound will be sedimented at the bottom of the recipient and found to be a polycrystalline powder. Image taken from [18].

[18]Note that this isn't a one-step reaction. The total reaction is composed of several middle steps.

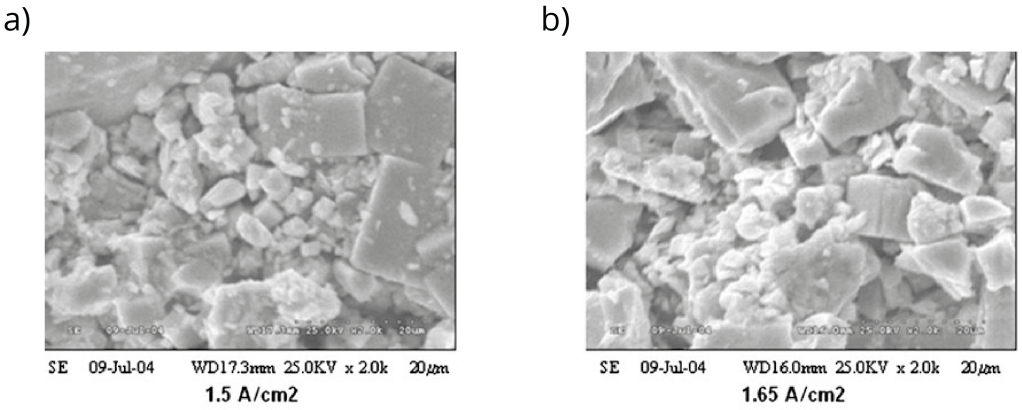

Figure 2.21. Scanning electron microscope (SEM) micrographs of different polycrystalline samples of SmB_6 generated by a) $1.5\,A/cm^2$ and b) $1.65\,A/cm^2$. Image taken from [8].

It is noteworthy that other growth techniques, such as the float method where the polycrystalline powder is heated up to its melting point and then cooled down while it crystallizes, can also be employed in the growth of SmB_6, yet, some experimental results, such as the possibility of finding one or a mix of atoms on its surface, depends on the technique employed in its development [34, 37]. Finally, at room temperature, the material has a considerably high conductivity, being classified as a semiconductor, and also has a positive Hall coefficient[19] [34].

Topology

In what follows, relying on literature, we analyzed two important experimental data regarding the triviality or non-triviality of SmB_6. First, for its resistivity, it was found the patterns shown in figure 2.22 for its bulk and surface, respectively. Note that as temperature decreases in (a) when we go from left to right, its bulk starts behaving as an insulator. On the other hand, as temperature goes down, its surface reaches a plateau of resistance that is characteristic of metals. This behavior is a strong indication that our material has a non-trivial topology, which could be easily explained recalling that topological insulators have surface-protected states that have such metallic nature. Finally, the Dirac-cone that precisely characterizes these surface-protected states and the non-triviality was found in 2.23. It is still important to note that the outlined linear

[19] It is interesting to note that since this coefficient is positive, we can't use semiclassical models, such as Drude's and Sommerfeld's, to study this material.

dispersion for the energy is called Dirac Cone due to its shape, and features a channel through which electrons can freely move without being scattered. Note, though, that these states are only found on the surface of the material.

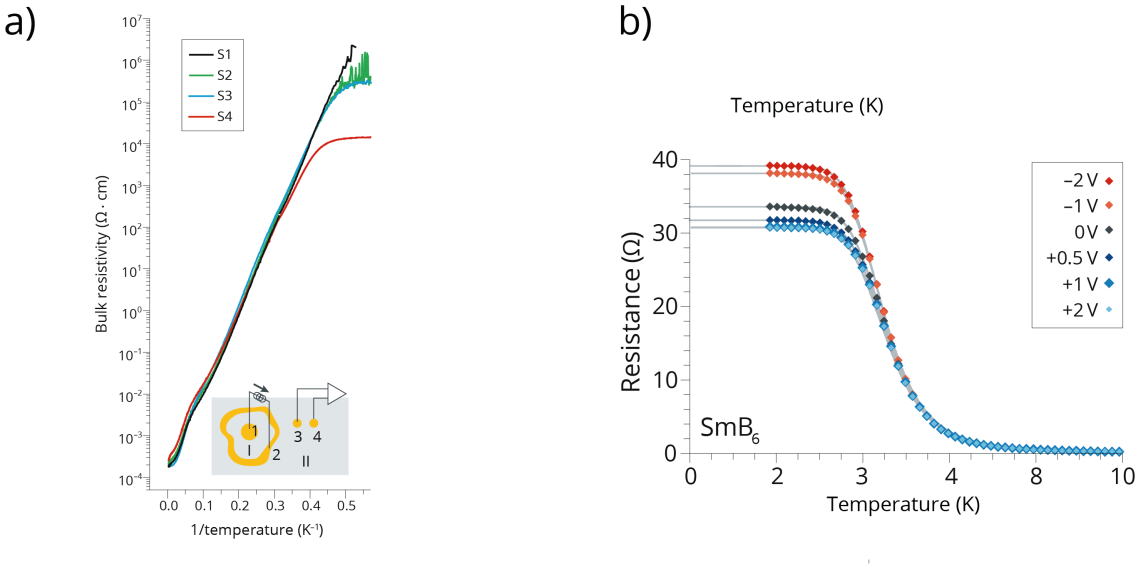

Figure 2.22. a) Temperature dependence of the resistivity of the bulk of SmB_6. b) Temperature dependence of the surface electrical resistance for different voltages. Image taken from [34].

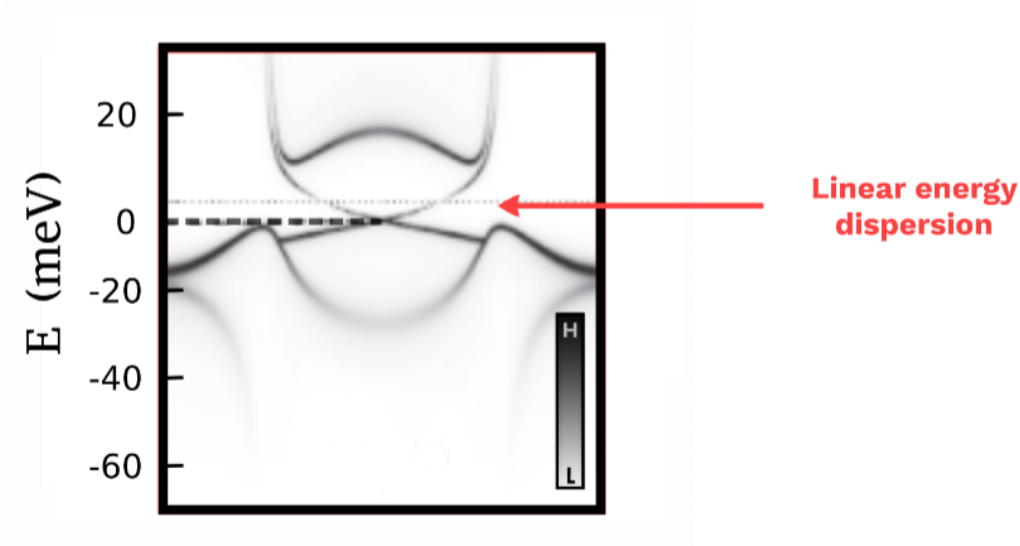

Figure 2.23. Average of the simulated spectral functions of SmB_6 surface states. Image taken from [37].

Chapter 3

Methodological Fundamentals

In this chapter, we will discuss the theoretical basis upon which this work was developed. To do that, we will start with the particle's wave function and its fundamental equation, then we will add other similar particles to our system and go over all approximations that are up to simplify or increase the accuracy of our study. This procedure will lead us to a largely known theory called DFT (density functional theory).

3.1 Born-Oppenheimer Approximation

When we go from the classic to the microscopic domain, we have that all Newton's laws give place to Schrodinger's equation, where such an expression can be promptly obtained from the former through the quantization rule [13]. For example, once the total energy of a classic particle subjected to a potential $\mathrm{V}(\mathbf{r})$ can be written as [53]:

$$\frac{p^2}{2m} + V(\mathbf{r}) = E, \tag{3.1}$$

we consequently have that its Schrodinger's equation will be given by:

$$\left[\frac{\hat{\mathbf{p}}^2}{2m} + V(\hat{\mathbf{r}})\right] |\psi\rangle = E\,|\psi\rangle \tag{3.2}$$

where $|\psi\rangle$ is a physical descriptor known as the particle's quantum state. Then, all greatnesses related to our system are gotten through this state by means of the employment of the quantum

mechanic postulates [13]. In what follows, to find out what $|\psi\rangle$ looks like, we may work on either the real or on the momentum space, when we will be finally able to pick up a face for both operators, $\hat{\mathbf{p}}$ and $\hat{\mathbf{r}}$. Despite that, and regardless of our choice, we will end up dealing with a differential equation that may or may not have an analytic solution.

Finally, that would be wonderful if all equations could be solved as precisely as we wanted, but it is worth noting that it actually gets way harder as we bring other particles to play because they start interacting among themselves, and the differential equation we are handling becomes analytically unsolvable. The point here is that there is no need to go too far to reach this condition because such an expression can only be analytically solved for two interacting particles [14, 53]. Bearing that in mind and including the fact we are studying solids, we may promptly realize that we are parsing several interacting electrons in such a way that we must, indeed, look for a method to simplify and turn it into something that can be used to predict the properties of the system without a heavy computational cost or, if possible, analytically. That's where the Born-Oppenheimer approximation comes in.

The Born-Oppenheimer approximation consists of regarding the nuclei and the electrons by different equations. Note that it isn't what we had at first, though, because both entities are indeed interacting with each other, but it is also quite reasonable because their masses are pretty different, in such a way that a nucleus *feels* its environment much weaker than an electron does and, in the limit where the electrons' masses tend to 0, we would have that all their movements would no longer depend on the electrons' [9]. Let's see how it shows up in calculus.

Considerations and Deduction

When we are dealing with an isolated multi-body problem, we know that its Hamiltonian is simply given by [23, 33]:

$$H_T = T_e + T_n + V_{ee} + V_{nn} + V_{en} \tag{3.3}$$

where we have the following correspondence for the subscripts used above: electrons (e), nuclei (n), electron-electron (ee), and electrons-nuclei (en). These terms, together, compose the eigenvalue equation for our system, which is simply:

$$\hat{\mathbf{H}}(\mathbf{r}, \mathbf{R})\Psi(\mathbf{r}, \mathbf{R}) = E\Psi(\mathbf{r}, \mathbf{R}) \tag{3.4}$$

where $\mathbf{r} = (\mathbf{r}_1, \mathbf{r}_2, \mathbf{r}_3, ...)$ denotes the positions of the electrons, and $\mathbf{R} = (\mathbf{R}_1, \mathbf{R}_2, \mathbf{R}_3, ...)$ represents the nuclei. Moreover, each term in equation 3.3 stands for a slice of the system's total energy and can, in Hartree units, be written as follows [13]:

- Nuclear kinetic energy:

$$\hat{\mathbf{T}}_N = -\sum_A \frac{1}{2M_A}\nabla_A^2 \tag{3.5}$$

- Electric potential energy among the nuclei:

$$\hat{\mathbf{V}}_{nn} = \sum_A \sum_{B>A} \frac{Z_A Z_B}{|\mathbf{R}_A - \mathbf{R}_B|} \tag{3.6}$$

- Electronic kinetic energy:

$$\hat{\mathbf{T}}_e = -\sum_i \frac{1}{2}\nabla_i^2 \tag{3.7}$$

- Electric potential energy among the electrons:

$$\hat{\mathbf{V}}_{ee} = \sum_i \sum_{j>i} \frac{1}{|\mathbf{r}_i - \mathbf{r}_j|} \tag{3.8}$$

- Electric potential energy among the nuclei and the electrons:

$$\hat{\mathbf{V}}_{ne} = -\sum_i \sum_A \frac{Z_A}{|\mathbf{R}_A - \mathbf{r}_i|} \tag{3.9}$$

The first approximation is based on the idea that the nuclei barely feel any interactions; in other words, they are approximately static in space. Consequently, the total wave function of our system may be pointed out as follows:

$$\Psi(\mathbf{r}, \mathbf{R}) = \Psi_e(\mathbf{r}, \mathbf{R})\Psi_n(\mathbf{R}) \tag{3.10}$$

where Ψ_e stands for the quantum state of all electrons, while Ψ_n denotes the nuclei. We may now replace this *ansatz* for Ψ and the extended expression for H_T into equation 3.4 to obtain:

$$(\hat{\mathbf{T}}_n + \hat{\mathbf{T}}_e + \hat{\mathbf{V}}_{ne} + \hat{\mathbf{V}}_{nn} + \hat{\mathbf{V}}_{ee})\Psi_e(\mathbf{r}, \mathbf{R})\Psi_n(\mathbf{R}) = E\Psi_e(\mathbf{r}, \mathbf{R})\Psi_n(\mathbf{R}) \tag{3.11}$$

Therefrom, applying the distributive on the left side, we get:

$$\hat{\mathbf{T}}_n\Psi_e\Psi_n + \hat{\mathbf{T}}_e\Psi_e\Psi_n + \hat{\mathbf{V}}_{ne}\Psi_e\Psi_n + \hat{\mathbf{V}}_{nn}\Psi_e\Psi_n + \hat{\mathbf{V}}_{ee}\Psi_e\Psi_n = E\Psi_e\Psi_n \tag{3.12}$$

Now, as aforementioned, regarding the kinetic energy of the nuclei, we have that at low temperatures $\mathrm{T}_e >> \mathrm{T}_n$ [54]. It enables us to say:

$$\hat{\mathbf{T}}_n\Psi_e\Psi_n \approx \Psi_e\hat{\mathbf{T}}_n\Psi_n \tag{3.13}$$

Such a statement is known as adiabatic approximation. We may now rearrange the terms in 3.12 according to the ones in 3.13 to obtain:

$$\Psi_e\hat{\mathbf{T}}_n\Psi_n + \Psi_n\hat{\mathbf{T}}_e\Psi_e + \left(\hat{\mathbf{V}}_{ne} + \hat{\mathbf{V}}_{nn} + \hat{\mathbf{V}}_{ee}\right)\Psi_e\Psi_n = E\Psi_e\Psi_n \tag{3.14}$$

Dividing both sides by $\Psi_e\Psi_n$:

$$\frac{1}{\Psi_n}\hat{\mathbf{T}}_n\Psi_n + \frac{1}{\Psi_e}\hat{\mathbf{T}}_e\Psi_e + \hat{\mathbf{V}}_{ne} + \hat{\mathbf{V}}_{nn} + \hat{\mathbf{V}}_{ee} - E = 0 \tag{3.15}$$

We may still rearrange it as:

$$\frac{1}{\Psi_e}\hat{\mathbf{T}}_e\Psi_e + \left(\hat{\mathbf{V}}_{ne} + \hat{\mathbf{V}}_{nn} + \hat{\mathbf{V}}_{ee}\right) = E - \frac{1}{\Psi_n}\hat{\mathbf{T}}_n\Psi_n = E(\mathbf{R}) \tag{3.16}$$

Finally, to evaluate this expression, we have to parse each of the following equations separately, which simply means that we have to solve the following eigenvalue equation:

$$\left[\hat{\mathbf{T}}_e + \hat{\mathbf{V}}_{ne} + \hat{\mathbf{V}}_{nn} + \hat{\mathbf{V}}_{ee}\right]\hat{\mathbf{\Psi}}_\mathbf{e} = \hat{\mathbf{H}}_e\Psi_e(\mathbf{r},\mathbf{R}) = E(\mathbf{R})\Psi_e(\mathbf{r},\mathbf{R}) \tag{3.17}$$

for the electrons and this one

$$\left[\hat{\mathbf{T}}_n + E(\mathbf{R})\right]\Psi_n(\mathbf{R}) = \hat{\mathbf{H}}_n\Psi_n(\mathbf{R}) = E\Psi_n(\mathbf{R}) \tag{3.18}$$

for the nuclei [54].

3.2 Variational Method

Even though the Born-Oppenheimer approximation has enabled us to simplify Schrodinger's equation for a complex system, we are still likely to deal with an analytically unsolvable equation. Hence, we must keep looking for either other approximations or methods to solve it as precisely as possible. This way, we could talk about iterative and perturbation approaches and, if our quantum system is at its lowest energy level, the variational method [5, 14, 21].

We know that every quantum-bonded system has negative, discrete, and well-defined energies; whence, using Born's postulate [17], we have that [14, 42]:

$$\frac{\langle \Psi | \hat{\mathbf{H}} | \Psi \rangle}{\langle \Psi | \Psi \rangle} \geqslant \epsilon_0 \tag{3.19}$$

whenever our system is at its lowest energy state. Note that it is true for any given $|\Psi\rangle$ and the corresponding Hamiltonian $\hat{\mathbf{H}}$. This statement basically stands for the existence of a fundamental energy level and it is also the heart of the variational method. Lastly, if we know ϵ_0 and $\hat{\mathbf{H}}$, we can come up with an *ansatz*[1] for $|\Psi\rangle$ and set it up so that the right side approaches the most to ϵ_0. Therefrom, such a value will represent what function, among the *ansatz* family we have chosen, gets the closest to the real state of our system. Although we may feel like we can directly apply this method to any system at its ground state, finding the best *ansatz* may be a challenging task, and to overcome this issue, we will present and discuss the density functional theory (DFT) in the upcoming sections.

3.3 Density Functional Theory (DFT)

As discussed previously, despite having the Born-Oppenheimer approximation, equation 3.17 is still analytically unsolvable and has a huge computational cost, forcing us to search for new methods to attack the problem of an isolated quantum multi-body system. Following this track, we could go over the Hartree-Fock (HF) approach, which starts throwing all electron-electron interactions away and turns our N-coupled equations into N uncoupled, one for each electron

[1] Such *ansatz* is just a function that obeys all boundaries conditions and depends on a yet unknown parameter α.

[21]. On the other hand, we know that this correlation among the electrons has a massive significance when we get away from the alkaline metals because their orbitals don't have the shape of a perfect sphere anymore, and it accounts for important electromagnetic and directional effects [5] that gives rise, for example, to the hydrogen bond as can be seen below:

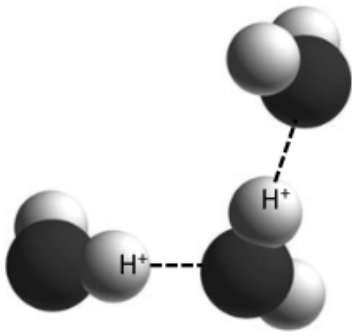

Figure 3.1. Hydrogen bonds in H_2O. The non-spherical shape of the orbitals gives rise to directional bindings and the only way we have to take it into consideration is by employing quantum mechanics, which leaves semi-classical models, such as Drude's and Sommerfeld's, behind [5]. On the other hand, some nuances show up in the process and make it a little harder to deal with. Image taken from [51].

This way, we still have the problem of how to handle a quantum multi-body system without losing its information. Fortunately, Hohenberg and Kohn, in 1964, almost fully answered this question with two theorems of great importance in which they proved that, instead of dealing with all those coupled equations, we could take the electronic density $\rho(\mathbf{r})$ as the system's fundamental variable[2] [25]. In other words, for systems at their ground state, $\rho(\mathbf{r})$, which only depends on 3 spatial coordinates, has the same amount of information as $\Psi(\mathbf{r})$, which, in its turn, involves 3N spatial coordinates, besides the electronic spin. Despite that, a way to find it explicitly was only published in 1965 by Kohn and Sham [32].

3.3.1 Hohenberg-Kohn Theorems

One of the biggest problems with the eigenvalue equation 3.17, besides its multi-body nature, is that we don't know what those potentials look like yet, thereby, if we manage to determine

[2] A great digress of what are fundamental variables is found in [50].

them, half of the job would get done, and we would only be left with the numerical part.

Hohenberg and Kohn proved that if we know the electronic density within a material at its ground state, we can promptly get the total potential, called v_{ext}, by means of a functional. In other words, if our system is at its ground state, $\rho(\mathbf{r})$ determines v_{ext} unambiguously, which, by its turn, determines $\hat{\mathbf{H}}_e$. It can be schematically shown by [25, 42]:

$$\rho(\mathbf{r}) \longrightarrow v_{ext} \longrightarrow \hat{\mathbf{H}} \longrightarrow \Psi \Longleftrightarrow \text{system's state}$$

from which we get

$$\epsilon_0 = E[\rho(\mathbf{r})]$$

The most mindful of you may be pointing out at this moment that it hasn't taken us really far yet because we still have no clues about what $\rho(\mathbf{r})$ looks like. However, here comes the second theorem of Hohenberg and Kohn, which indeed turns it all into a very useful development. First, remember that if we are studying a system at its ground state, then its total energy must be the lowest allowed one and we can make good use of the variational method. Furthermore, we have just seen that the system's total energy is given by a functional of the electronic density, denoted as $E[\rho(\mathbf{r})]$. We may then gather it all into the following statement:

$$E[\rho(\mathbf{r})] \geq E[\rho_0(\mathbf{r})] = E_0 \tag{3.20}$$

which briefly represents the second theorem of Hohenberg and Kohn [25, 42]. In short, for systems at their ground state, the closer our function for $\rho(\mathbf{r})$ gets to their real one, ρ_0, the closer the functional $E[\rho(\mathbf{r})]$ gets to E_0.

These two theorems allow us to use $\rho(\mathbf{r})$ to study a multi-body quantum system and present a method to verify the accuracy of our solution. However, they do not detail a streamlined and optimized iterative process to achieve this goal. The subsequent development, presented below, addresses this gap and outlines an approach to accomplish it.

3.3.2 Kohn-Sham Equation

Since energies are scalars and ρ is now our fundamental variable, we can set[3], in Hartree units, the total energy of our system as:

$$E[\rho(\mathbf{r})] \equiv E_{ext}[\rho(\mathbf{r})] + E_{Hartree}[\rho(\mathbf{r})] + G[\rho(\mathbf{r})] \tag{3.21}$$

where [21, 42]:

- The first term arises from the external potential $v_{ext}(\mathbf{r})$ and is given by:

$$E_{ext}[\rho] = \int v(\mathbf{r})\rho(\mathbf{r})d\mathbf{r} \tag{3.22}$$

- The second one is the classical electrostatic energy (Hartree's term):

$$E_{Hartree}[\rho] = \frac{1}{2}\int\int \frac{\rho(\mathbf{r})\rho(\mathbf{r}')}{|\mathbf{r}-\mathbf{r}'|}d\mathbf{r} \tag{3.23}$$

- The last item includes the energy of the non-interacting system, $T[\rho(\mathbf{r})]$, the unknown exchange-correlation energy, $E_{xc}[\rho(\mathbf{r})]$, and can be written as:

$$G[\rho(\mathbf{r})] \equiv T[\rho(\mathbf{r})] + E_{xc}[\rho(\mathbf{r})] \tag{3.24}$$

Finally, while E_{xc} is a complementary and unknown energy due to the fermionic nature of the electrons, $T[\rho(\mathbf{r})]$ is gotten through:

$$T[\rho(\mathbf{r})] = -\frac{1}{2}\sum_{i}^{N}\int \psi_i^*(\mathbf{r})\nabla^2\psi_i(\mathbf{r})d(\mathbf{r}) \tag{3.25}$$

We may still define electronic density as [13, 25]:

$$\rho(\mathbf{r}) = \sum \psi_i^*(\mathbf{r})\psi_i(\mathbf{r}) \tag{3.26}$$

where the sum goes over all occupied states of our hypothetical system of N non-interacting

[3]The same way as $6 = 1 + 2 + 3$, we can also break down the energy as a sum of factors [53].

electrons. Making good use of Hohenberg-Kohn's theorem, we should now find out what density minimizes the energy of our system. To accomplish this, we might proceed by getting the difference between the total energy, $E[\rho(\mathbf{r})]$, with the contribution of each orbital ψ_i. In other words [21, 33, 42]:

$$\mathcal{L}[\rho] = E[\rho] - \sum_i \epsilon_i \int \psi_i^*(\mathbf{r})\psi_i(\mathbf{r})d\mathbf{r} \tag{3.27}$$

where ϵ_i is the energy related to the i-nth orbital. Now, once we are handling a system at its lowest energy level, its functional derivation with respect to small variations in ρ, which can be understood as small variations in ψ, must be zero. It then leads us to [21, 42]:

$$\begin{aligned}\frac{\delta\mathcal{L}}{\delta\psi_i^*(\mathbf{r})} &= \frac{\delta E[\rho]}{\delta\psi_i^*(\mathbf{r})} - \frac{\delta}{\delta\psi_i^*(\mathbf{r})}\sum_i \epsilon_i \int \psi_i^*(\mathbf{r})\psi_i(\mathbf{r})d\mathbf{r} \\ &= \frac{\delta}{\delta\psi_i^*(\mathbf{r})}\left(E_{ext}[\rho(\mathbf{r})] + E_{Hartree}[\rho(\mathbf{r})] + G[\rho(\mathbf{r})]\right) - \sum_i \epsilon_i \frac{\delta}{\delta\psi_i^*(\mathbf{r})}\int \psi_i^*(\mathbf{r})\psi_i(\mathbf{r})d\mathbf{r} = 0\end{aligned} \tag{3.28}$$

On the other hand, since ψ and ρ are related through 3.26, and all greatnesses within the former brackets above are functions of ρ, we can make good use of the chain rule for functionals [3]:

$$\frac{\delta F}{\delta\psi_i^*} = \frac{\delta F}{\delta n}\frac{\delta n}{\delta\psi_i^*} = \frac{\delta F}{\delta\psi_i^*}\frac{\delta(\psi_i^*\psi_i)}{\delta\psi_i^*} = \frac{\delta F}{\delta\psi_i^*}\psi_i \tag{3.29}$$

and the fact that G is given by $T + E_{ex}$, to rewrite 3.28 as:

$$\frac{\delta\mathcal{L}}{\delta\psi_i^*(\mathbf{r})} = \frac{\delta T}{\delta\psi_i^*(\mathbf{r})} + \frac{\delta}{\delta\rho(\mathbf{r})}\left(E_{ext} + E_{Hartree} + E_{ex}\right)\frac{\delta\rho(\mathbf{r})}{\delta\psi_i^*(\mathbf{r})} - \epsilon_i\psi_i^*(\mathbf{r}) = 0 \tag{3.30}$$

Wherefrom we can promptly obtain the following identities:

$$\frac{\delta T}{\delta\psi_i^*(\mathbf{r})} = -\frac{1}{2}\nabla^2\psi_i,\ \frac{\delta E_{ext}}{\delta\rho(\mathbf{r})} = v(\mathbf{r}),\ \frac{\delta E_{Hartree}}{\delta\rho(\mathbf{r})} = \int\frac{\rho(\mathbf{r})}{|\mathbf{r}-\mathbf{r}'|}d\mathbf{r},\quad \text{and}\quad \frac{\delta\rho(\mathbf{r})}{\delta\psi_i^*(\mathbf{r})} = \psi_i(\mathbf{r})$$

Finally, if we plug the right-hand values found above into 3.30, we reach:

$$\left[-\frac{1}{2}\nabla^2 + v_{ext}(\mathbf{r}) + \int\frac{\rho(\mathbf{r})}{|\mathbf{r}-\mathbf{r}'|}d\mathbf{r}' + \frac{\delta E_{xc}}{\delta\rho(\mathbf{r})}\right]\psi_i^{KS} = \epsilon_i\psi_i^{KS} \tag{3.31}$$

This expression is called Kohn-Sham equation[4] and was discovered in 1965 [32]. It is still worth noting that such an expression is quite similar to Schrödinger's equation for one particle with an effective potential given by [42]:

$$v_{ks}(\mathbf{r}) = v_{ext} + \int \frac{\rho(\mathbf{r})}{|\mathbf{r} - \mathbf{r}'|} d\mathbf{r}' + \frac{\delta E_{xc}}{\delta \rho(\mathbf{r})} \tag{3.32}$$

Despite that, we aren't handling only one particle anymore, but N of them; and we have also moved from 3N variables to N. On the other hand, we don't know what E_{ex} is like yet, but before making any digresses about it, let's outline how this equation works more deeply and how we use it to study solids.

Working with Kohn-Sham Equation

As it would have happened if we had started from scratch with Schrödinger's equation, we found ourselves with an unknown entity that is in the core of our development: E_{ex}. To overcome this challenge and make some progress toward a useful result, we need to adopt a specific approach. For this purpose, let's make an *ansatz* for ρ. This *ansatz* provides us with all the necessary information that was previously neglected, allowing us to solve the problem self-consistently. As we proceed with the solution, the missing information is gradually acquired and we can repeat the process iteratively until it either converges or diverges.

In practical terms, we make an *ansatz* for $\rho(\mathbf{r})$, let's say $\rho^j(\mathbf{r})$, plug it into expression 3.31 and solve it to find out all eigenstates ψ_i. Therefrom, we determine the system's electronic density again through 3.26 using these new eigenstates. If the found density is equal to the former, then we are done, otherwise, we repeat the process using the new density until the following criterion is satisfied: $\rho^j(\mathbf{r}) \approx \rho^{j+1}(\mathbf{r})$. This process is schematically shown in figure 3.2. Then, once convergence is achieved and the final Kohn-Sham orbitals are determined, we can promptly obtain the total electronic energy for the system using the following equation [21]:

$$E = \sum_i^N \epsilon_i - \frac{1}{2} \iint \frac{\rho(\mathbf{r})\rho(\mathbf{r}')}{|\mathbf{r} - \mathbf{r}'|} d\mathbf{r} d\mathbf{r}' - \int \frac{\delta E_{ex}}{\delta \rho(\mathbf{r})} \rho(\mathbf{r}) d\mathbf{r} - E_{ex}[\rho(\mathbf{r})] \tag{3.33}$$

However, it is important to note that we are currently uncertain about the precise form of E_{ex}.

[4] The superscript KS stands for Kohn-Sham.

To address this issue, further investigation and alternative approaches will be discussed in more detail in the upcoming sections.

Steps of Kohn-Sham Self-Consistent Procedure

1. **Ansatz for $\rho(\mathbf{r})$:**

$$\rho(\mathbf{r}) \rightarrow \text{Initial guess}$$

2. **Formulate the Kohn-Sham Hamiltonian:**

$$H_{\text{KS}} = -\frac{\nabla^2}{2m} + V_{\text{ext}}(\mathbf{r}) + V_{\text{H}}(\mathbf{r}) + V_{\text{xc}}(\mathbf{r})$$

3. **Solve Kohn-Sham's Equations:**

$$H_{\text{KS}}\psi_i(\mathbf{r}) = \varepsilon_i\psi_i(\mathbf{r})$$

4. **Update Electronic Density:**

$$\rho(\mathbf{r}) = \sum |\psi_i(\mathbf{r})|^2$$

5. **Convergence Check:**

Check for convergence by comparing the updated electronic density $\rho(r)$ with the previous iteration's density.

If the difference is below a predefined threshold, the procedure has converged, and the self-consistent calculation is complete.

Otherwise, return to step 2.

6. **Finalize:**

Once convergence is achieved, the final Kohn-Sham orbitals $\psi_i(\mathbf{r})$ and electronic density $\rho(\mathbf{r})$ represent the self-consistent solution for the electronic structure of the system.

Figure 3.2. Kohn-Sham's general algorithm [21].

3.4 Density Approximations

Recall that the standard approach for dealing with many-electron systems involves breaking them down into smaller components, analyzing each component individually, and then combining

the results. For example, as mentioned previously, the total energy of a quantum multi-body system may be gotten through the following functional:

$$E[\rho(\mathbf{r})] = T_R + V_{ext} + E_H + E_x + E_c \tag{3.34}$$

where we went a little farther than before and divided E_{xc} into E_x, the exchange energy, and E_c, the correlation energy among electrons. The main problem here is that we haven't determined a face for these two functionals yet. Then, our first challenge is to determine a nature and a face to H_c, which can be done by noting that it arises from the fact that E_H accounts for all states at all positions, while, on the other hand, that can't happen because we can't distinguish electrons once they have no dimension and are all equal to each other, in short, because of Pauli's exclusion principle [17]. Consequently, we need to find an expression that regards all contributions violating it. As a direct result, such an expression must resemble E_H, but with the constraint that it only accounts for two states occupying the same position in space at the same time. Following that reasoning, Kohn and Sham, in 1965, proposed to consider all electrons in any material as being locally homogeneous so that we could disregard effects not related to Pauli's exclusion principle and focus ourselves on the exchange energy itself [31]. Note, though, that such homogeneity is left behind at the end when we integrate all greatnesses. This approach, called Local Density Approximation (LDA), involves considering individual regions, represented by tiny boxes taken from the material as depicted in figure 3.3, calculating the amount of energy that violates Pauli's principle, and then replicating the procedure for the entire space through integrals.

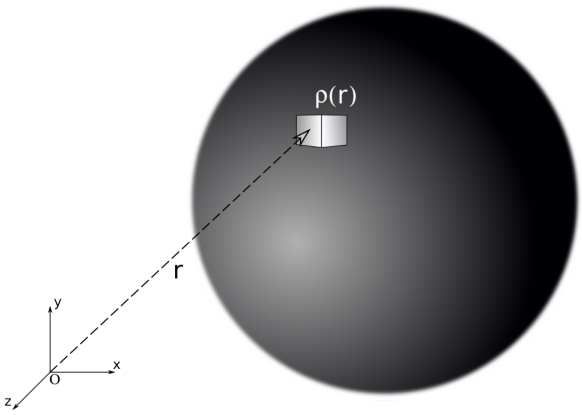

Figure 3.3. Differential box with a free electron gas and electronic density $\rho(\mathbf{r})$ used to study the exchange energy [42].

Lastly, it turns out to be a very useful approach because it leads us to handle a homogeneous gas of electrons, for which we can find H_x exactly and look for H_c numerically afterward.

3.4.1 Exchange Energy of the Free Electron Gas within the LDA

The free electron gas is the simplest model of electrons in a solid because they are assumed to not interact with each other and are subjected to a constant external potential which can be set to zero for convenience [5, 21]. Under these ideas, its Hamiltonian is simply given by:

$$\left[\frac{\hat{\mathbf{p}}^2}{2m} + \cancel{V(\hat{\mathbf{r}})}\right]|\psi\rangle = E\,|\psi\rangle \tag{3.35}$$

while its eigenstates and eigenvalues are, respectively [13, 17]:

$$\psi_k(\mathbf{r}) = \frac{1}{\sqrt{V}}\exp\{i\mathbf{k}\cdot\mathbf{r}\} \quad \text{and} \quad \epsilon_k = \frac{|\mathbf{k}|^2}{2} \tag{3.36}$$

where V is the volume of the whole system, which, in our case, is the tiny box. Moreover, notice that once it doesn't take time into consideration, these solutions stand for stationary states with wavevectors $\mathbf{k}$. Moreover, when handling a gas of free electrons, we can keep in mind that all greatnesses only rely upon the electronic density, for instance, its Fermi wavevector[5] is given by [21]:

$$k_F = (3\pi^2 n)^{\frac{1}{3}} \tag{3.37}$$

Finally, recalling the discussion we have had previously, the exchange energy must resemble $H_{Hartree}$, but it must only treat the special case where electrons in different states occupy the same region in space at the same time. Therefrom, if there is no net magnetic moment, it may be achieved through the following expression:

$$\iint_V \frac{\psi_i^*(\mathbf{r})\psi_i(\mathbf{r}')\psi_j^*(\mathbf{r}')\psi_j(\mathbf{r})}{|\mathbf{r}-\mathbf{r}'|}d\mathbf{r}'d\mathbf{r} \tag{3.38}$$

It is still worth noting that these two states, i and j, are distributed over the same region, which is what we wanted at first. Besides, since all states must be considered and each state must have

[5] It is the wavevector related to the highest occupied state.

two electrons to deliver a zero net magnetic moment system, we need to sum over all i, j, and multiply it by 2. However, to avoid counting the same state twice when we go from (i,j) to (j,i), we must also divide it by two. Therefore, the exact expression for the exchange energy of a free electron gas in LDA is [21]:

$$E_x = -\cancel{2}\frac{1}{\cancel{2}}\sum_i \sum_j \iint_V \frac{\psi_i^*(\mathbf{r})\psi_i(\mathbf{r}')\psi_j^*(\mathbf{r}')\psi_j(\mathbf{r})}{|\mathbf{r}-\mathbf{r}'|} d\mathbf{r}' d\mathbf{r} \tag{3.39}$$

In our case, since free electrons aren't bonded to anything, their eigenvalues build up a continuous spectrum. Consequently, it forces us to replace the sums over the occupied states by integrals over the wavevectors, in other words [3]:

$$\sum_i \longrightarrow \frac{V}{(2\pi)^3}\int_{|\mathbf{k}|\leq k_F} d\mathbf{k} \tag{3.40}$$

Now, if we use it, plus the results written in 3.36, we may promptly find:

$$\begin{aligned} E_x &= \frac{V}{(2\pi)^3}\int_{|\mathbf{k}|\leq k_F} d\mathbf{k} \frac{V}{(2\pi)^3}\int_{|\mathbf{k}'|\leq k_F} d\mathbf{k}' \iint_V \frac{\frac{1}{\sqrt{V}}e^{-i\mathbf{k}\cdot\mathbf{r}}\frac{1}{\sqrt{V}}e^{i\mathbf{k}\cdot\mathbf{r}'}}{|\mathbf{r}-\mathbf{r}'|} \times \cdots \\ &\qquad \cdots \times \frac{\frac{1}{\sqrt{V}}e^{-i\mathbf{k}'\cdot\mathbf{r}'}\frac{1}{\sqrt{V}}e^{i\mathbf{k}'\cdot\mathbf{r}}}{1} d\mathbf{r}' d\mathbf{r} \\ &= \frac{\cancel{V^2}}{(2\pi)^6\cancel{V^2}}\int_{|\mathbf{k}|\leq k_F} d\mathbf{k} \int_{|\mathbf{k}'|\leq k_F} d\mathbf{k}' \iint_V \frac{e^{-i\mathbf{k}\cdot(\mathbf{r}-\mathbf{r}')}e^{i\mathbf{k}\cdot(\mathbf{r}-\mathbf{r}')}}{|\mathbf{r}-\mathbf{r}'|} d\mathbf{r}' d\mathbf{r} \\ &= \frac{1}{(2\pi)^6}\int_{|\mathbf{k}|\leq k_F} d\mathbf{k} \int_{|\mathbf{k}'|\leq k_F} d\mathbf{k}' \iint_V \frac{e^{-i(\mathbf{k}-\mathbf{k}')\cdot(\mathbf{r}-\mathbf{r}')}}{|\mathbf{r}-\mathbf{r}'|} d\mathbf{r}' d\mathbf{r} \end{aligned}$$

This expression appears to be quite complex at first glance, but with some convenient changes of variables, its evaluation becomes manageable. Initially, it is worth noting that only the relative position between two electrons, denoted as $\mathbf{r}-\mathbf{r}'$, is present. Secondly, we can simplify the problem by introducing dimensionless variables, scaling the wavevectors with k_F and the positions with k_F^{-1}. As a result, the new changes in variables are as follows:

$$\mathbf{u} = k_F(\mathbf{r}-\mathbf{r}'), \quad \mathbf{q} = \frac{\mathbf{k}}{k_F}, \quad \mathbf{q}' = \frac{\mathbf{k}'}{k_F} \tag{3.41}$$

while the corresponding changes in the volume elements are [21]:

$$d\mathbf{r}' = \frac{d\mathbf{u}}{k_F^3}, \quad d\mathbf{k} = k_F^3\, d\mathbf{q}, \quad d\mathbf{k}' = k_F^3\, d\mathbf{q}' \tag{3.42}$$

Hence, plugging these values into our initial expression and considering $\int d\mathbf{r} = V$, we find:

$$\begin{aligned} E_x &= \frac{1}{(2\pi)^6} \int_{|\mathbf{q}|\leq 1} k_F^3\, d\mathbf{q} \int_{|\mathbf{q}'|\leq 1} k_F^3\, d\mathbf{q}' \int_V d\mathbf{r} \int \frac{\mathrm{e}^{-i(\mathbf{q}-\mathbf{q}')\cdot\mathbf{u}}}{|\frac{\mathbf{u}}{k_F}|} \frac{d\mathbf{u}}{k_F^3} \\ &= \frac{k_F^4}{(2\pi)^6} \int_{|\mathbf{q}|\leq 1} d\mathbf{q} \int_{|\mathbf{q}'|\leq 1} d\mathbf{q}' \int \frac{\mathrm{e}^{-i(\mathbf{q}-\mathbf{q}')\cdot\mathbf{u}}}{|\mathbf{u}|} d\mathbf{u} \end{aligned} \tag{3.43}$$

or simply:

$$E_x = -\frac{C}{(2\pi)^6} k_F^4 V \tag{3.44}$$

where C is a numerical dimensionless constant given by [21]:

$$C = \int_{|\mathbf{q}|\leq 1} d\mathbf{q} \int_{|\mathbf{q}'|\leq 1} d\mathbf{q}' \int \frac{\mathrm{e}^{-i(\mathbf{q}-\mathbf{q}')\cdot\mathbf{u}}}{|\mathbf{u}|} d\mathbf{u} \tag{3.45}$$

In the assessment of this constant, the final integral on the right-hand side is computed as V approaches infinity. The explicit evaluation of the constant C can be accomplished through a geometric construction, yielding the result of $16\pi^3$ [21]. If we plug this term and expression 3.37 into function 3.44, we achieve the expression below for E_x (in Hartree units):

$$\begin{aligned} E_x &= -\frac{16\pi^3}{(2\pi)^6} \left[(3\pi^2 n)^{\frac{1}{3}}\right]^4 V \\ &= \frac{1}{4\pi^3} 3\pi^2 (3\pi)^{\frac{1}{3}} n^{\frac{4}{3}} V \\ &= -\frac{3}{4} \left(\frac{3}{\pi}\right)^{\frac{1}{3}} n^{\frac{3}{4}} V \end{aligned} \tag{3.46}$$

It concludes our discussion regarding exchange energies within the local density approximation. It is worth noting that nothing has been said about spins and excited states yet. A brief explanation about it will be given in the upcoming subsections.

3.4.2 Correlation Energy of the Free Electron Gas within the LDA

On the other hand, in contrast to the exchange energy, there isn't an analytic way to assemble the correlation energy for electronic systems. Despite that, since we have already found E_x, we can get it numerically for a free electron gas by solving the many-particle Schrödinger's equation with stochastic numerical methods as Cerpeley and Alder did in 1980 [12].

The correlation energy of the electron gas can be determined by subtracting the known contributions of kinetic, Hartree, and exchange energies from the total energies calculated by Ceperley and Alder. The data obtained by them was then reformulated into a parametrized form by Perdew and Zunger in 1981 [44], and the resulting expression, in the scenario of zero net magnetic moments, is given by:

$$E_C = nV \begin{cases} 0.0311 \ln r_s - 0.0480 + 0.002 r_s \ln r_s - 0.0116 r_s & \text{if} \quad r_s < 1 \\ \dfrac{-0.1423}{1 + 1.0529\sqrt{r_s} + 0.3334 r_s} & \text{if} \quad r_s \geq 1 \end{cases} \tag{3.47}$$

where

$$\frac{V}{N} = \frac{4\pi}{3} r_s^3 = \frac{1}{n} \tag{3.48}$$

and r_s is the Wigner-Seitz radius [21].

3.4.3 More Real Materials

Even though we have reached a round expression for electronic states and the total energy in a solid, it must be noticed that we haven't taken systems with spin, as well as excited states into consideration yet, and that would certainly make all our reasoning a little more real. The point here is that it can't be achieved with the standard DFT because considering spins, for example, changes the main Hamiltonian from:

$$\hat{\mathbf{H}} = \hat{\mathbf{T}} + \hat{\mathbf{V}}_{ee} + \sum_i v(\mathbf{r}_i) \tag{3.49}$$

to

$$\hat{\mathbf{H}} = \hat{\mathbf{T}} + \hat{\mathbf{V}}_{ee} + \sum_i v(\mathbf{r}_i) - 2\mu \sum_i B(\mathbf{r}_i)\, \hat{\mathbf{s}}_z^i \tag{3.50}$$

where $v(\mathbf{r})$ and $B(\mathbf{r})$ are external scalar and magnetic fields (the latter couples to electron spin), respectively, and $\hat{\mathbf{T}}$ is the kinetic energy operator [44]. In turn, it implies changes in all states and, consequently, the energy of the system. In the same way, our subsequent LDA must also take the spin into account becoming then the local spin density theory (LSDA)[6]. On the other hand, considering excited states isn't allowed by Kohn-Sham's theory the way it was stated here because it relies upon the variational method[7]. One way to change directions and take it into account consists of replacing the electronic density by:

$$\rho(\mathbf{r}) = \sum_i \eta_i |\psi_i(\mathbf{r})|^2 \tag{3.51}$$

where η_i stands for an occupation number for each of the electronic states [28]. This way, for a given set of η_i, the self-consistent solution would lead us to:

$$\bar{E} = \bar{T} + U[\rho] + E_{xc}[\rho] \tag{3.52}$$

Nevertheless, although it is well-defined mathematically, in general, $\bar{E}$ isn't equal to the total energy E. However, when ρ_i has the form of the Fermi-Dirac distribution, $\bar{E}$ becomes numerically equal to E by construction [28]. At last, once LDA is all based on a free electron gas, it would be expected to work better for more homogeneous systems such as metals, in which the electronic density doesn't change heavily in space. Despite that, it fits pretty well most atomic, crystal, and molecular systems, once the region we are studying isn't right over the nuclei and ρ is smoothly spread over space [42]. Despite that, LDA has its constraints and other approaches have been developed through the last decades to overcome them. In the next section, we will briefly discuss one of them, namely, the general gradient approximation (GGA).

3.4.4 General Gradient Approximation (GGA)

Besides its excellent fit, when the electronic charge within a solid system varies heavily over a region, the local density approach, as the LSDA, doesn't depict the system accurately anymore once its basis becomes weak due to the high inhomogeneity in ρ. One way to bypass this issue and

[6] It is generally used to study systems where spin polarization is considered.
[7] We have only dealt with the ground state so far.

restore a strong basis for studying the system consists of including a variation in ρ by means of its gradient in our development, which stands for the heart of the General Gradient Approximation (GGA) [42]. Following this reasoning, we may properly address this question through the following function:

$$E_{xc}[\rho] \equiv E_{xc}^{GGA}[\rho(\mathbf{r})] = \int \rho(\mathbf{r})\epsilon_x^{unif}\rho(\mathbf{r})F_{xc}(\rho(\mathbf{r}), \nabla\rho(\mathbf{r}))\, d\mathbf{r} \tag{3.53}$$

where ϵ_x^{unif} is the exchange energy gotten with LDA and F_{xc} is an enhancement factor used to rescale the local energy according to GGA [43]. For comprehension's sake, in table 3.1, we rewrote some data from [43] that intends to show how more accurate the present approach is regarding the former LSDA.

System	ΔE^{UHF}	ΔE^{LSD}	ΔE^{PW91}	ΔE^{PBE}	ΔE^{expt}
H_2	84	113	105	105	109
LiH	33	60	53	52	58
CH_4	328	462	421	420	419
NH_3	201	337	303	302	297
OH	68	124	110	110	107
H_2O	155	267	235	234	232
HF	97	162	143	142	141
Li_2	3	23	20	19	24
LiF	89	153	137	136	139
Be_2	-7	13	10	10	3
C_2H_2	294	460	415	415	405
C_2H_4	428	633	573	571	563
HCN	199	361	326	326	312
CO	174	299	269	269	259
N_2	115	267	242	243	229
NO	53	199	171	172	153
O_2	33	175	143	144	121
F_24	-37	78	54	53	39
P_2	36	142	120	120	117
Cl_2	17	81	64	63	58
Mean abs. error	71.2	31.4	8.0	7.9	...

Table 3.1. Atomization energies of molecules in kcal/mol (1eV $\neq$ 23.06 kcal/mol). E_{xc} were evaluated on self-consistent densities at experimental geometries. Nonspherical densities and Kohn-Sham potentials were used for open-shell atoms. The experimental values for DE (with zero point vibration removed) were taken from [15]. PBE is the simplified GGA, while UHF is unrestricted Hartree-Fock, for comparison. All data was taken from [43].

3.5 Pseudopotentials

Whenever we are talking about crystals, in what concerns modern electronic calculations, it should be borne in mind that we are mainly chasing their valence states because they account for everything that happens inside the material, from electronic bonds to transition state barriers. Fortunately enough, systems under study have increased a lot over the past decades becoming quite large and complex, which in turn puts those simple models, such as Drude's and Sommerfeld's, within a very limited scope. On the other hand, other models, such as DFT, have been gaining more and more value over the years due to their basis on *first principles*[8] calculations [47]. In what follows, we consistently encounter either analytically unsolvable systems or the need to make approximations to turn the problem into something computationally manageable, leading us to the following questions: are we proceeding in the right direction? Are the results trustworthy? And if so, how can we know that?

DFT addresses some of the aforementioned problems by replacing real functions with unknown functionals that can be determined empirically or through a simple model, as previously done in the LDA (Local Density Approximation). Thus, when working with DFT, we are inherently relying on the following assumptions [47]:

1. All functionals are approximations;
2. No presently existing functional is highly accurate for all properties of interest;
3. Any functional can be applied to any electronic structure problem without requiring additional input;

In what follows, since we are solving the Kohm-Sham equation for the whole space and we are focusing on the valence electrons, we may also replace the real *all-electron* potential with a pseudopotential to diminish the computational cost of our study. This pseudopotential is equal to the real one inside the valence orbital and surely leads us to the same solution there. This procedure also gets rid of the high-frequency part of the electrons' wave functions that are found outside the valence orbital, which in turn enables us to use plane wave functions to represent Kohm-Sham

[8] At this moment, it is worth taking a break and looking up about the difference between phenomenological and constructive (*first principles*) models.

states because now a smaller number of them is needed [5, 42]. Finally, the pseudopotential and the pseudofunction may be schematically depicted as follows:

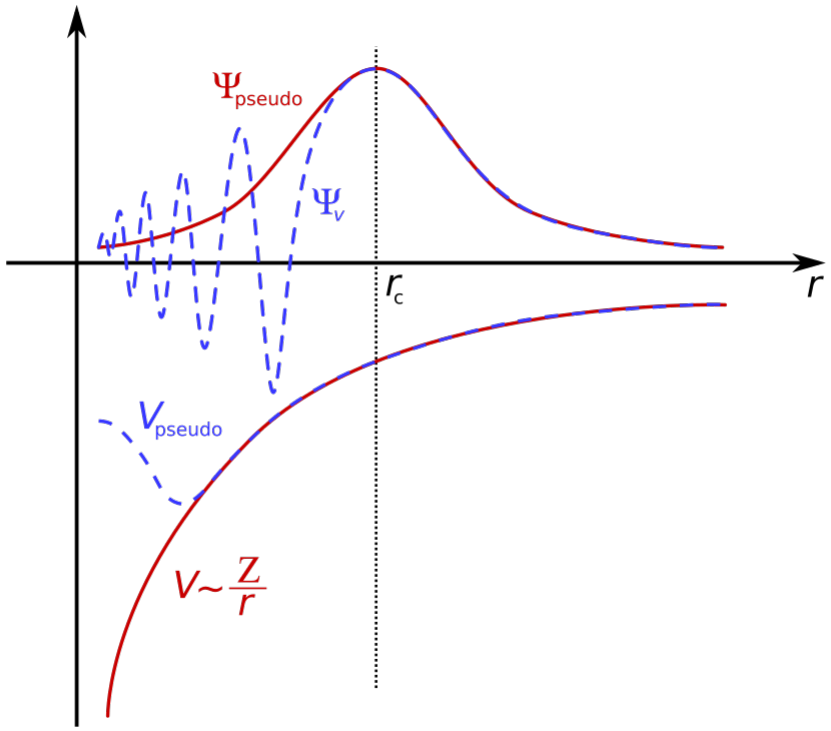

Figure 3.4. This figure presents the behavior of pseudofunctions and what they look like in general [42].

It is only due to the use of pseudopotentials that we can perform electronic studies with plane waves because we needed thousands of them at first, and that would require a huge and mostly intangible computational cost. Besides, note that we are indeed going in the right direction once plane waves promptly satisfy Bloch's theorem, furthermore, also note that our pseudofunction in the core is simply the reflection of the real plane wave, Ψ_V, through $\mathbf{r}_c$. At last, it is worth noting that functionals may be gotten through three different ways: empirically, semi-empirically, and non-empirically. Each of them has its own advantages and disadvantages as follows [47]:

- Empirically: has high precision, but can only be reliably used to study the system from which it was gotten;
- Semi-empirically: uses a few empirical parameters that experts have fitted. It can speed up the tests and is reliable for similar systems;

- Non-empirically: is developed from scratch, using only general rules of quantum mechanics and special conditions to determine the parameters;

This way, a reliable DFT should be thought of according to the following sequence [47]:

$$\text{ERROR (functional)} > \text{ERROR (basis set)} > \text{ERROR (Coulomb)} > \text{ERROR (grid)}$$

In the upcoming sections, we are discussing some non-empirical pseudopotentials and how we can manage to find them.

3.5.1 Orthogonalized Plane-Wave Method (OPW)

We can't manage to generate valence states *everywhere* with only a few plane waves because this procedure can't depict the high-frequency behavior found near the core region [42]. Despite that, Herring noted in 1940 that we could overcome this issue by using not only simple waves but plane waves that were *orthogonalized* to the core levels right from the start. Therefrom, using c and v for core and valence states, respectively, we can define the *orthogonalized* plane wave (OPW) ϕ_k by [5]:

$$\phi_{\mathbf{k}} = \mathrm{e}^{i\mathbf{k}\cdot\mathbf{r}} + \sum_c b_c\, \psi_{\mathbf{k}}(\mathbf{r}) \tag{3.54}$$

where the sum goes over all core levels with Bloch wavevector $\mathbf{k}$, and the core wavefunctions, ψ_k^c, are assumed to be known beforehand. Besides, the constants b_c are determined by demanding $\phi_{\mathbf{k}}$ to be orthogonal to every core level, which is given by:

$$\int d\mathbf{r}\, \psi_{\mathbf{k}}^{c*}(\mathbf{r})\, \phi_{\mathbf{k}}(\mathbf{r}) = 0 \tag{3.55}$$

which implies that

$$b_c = -\int d\mathbf{r}\, \psi_{\mathbf{k}}^{c*}(\mathbf{r})\, \mathrm{e}^{i\mathbf{k}\cdot\mathbf{r}} \tag{3.56}$$

Since each term in 3.54 satisfies Bloch's theorem, so does the entire expression for $\phi_{\mathbf{k}}$. On the other hand, the more we approach a lattice point, the more the latter term in 3.54 influences its behavior, while the farther we are from it, the more the former comes into play. Consequently, it does satisfy the Hamiltonian equation everywhere and we can search for the eigenstates that

are spanned by the following functions:

$$\psi_{\mathbf{k}} = \sum_{\mathbf{K}} c_{\mathbf{K}}\, \phi_{\mathbf{k}+\mathbf{K}} \tag{3.57}$$

3.5.2 Phillips and Kleiman

Firstly, we'd like to note that the pseudopotential theory, in its earliest formulation, was pretty much a reshaping of the OPW approach. Hence, a possible solution for valence states could be thought of as:

$$\psi^{v}_{\mathbf{k}}(\mathbf{r}) = \sum_{\mathbf{K}} c_{\mathbf{K}}\, \phi^{v}_{\mathbf{k}+\mathbf{K}} \tag{3.58}$$

which, according to 3.54, is simply [5]:

$$\begin{aligned}
\psi^{v}_{\mathbf{k}}(\mathbf{r}) &= \sum_{\mathbf{K}} c_{\mathbf{K}} \left[e^{i(\mathbf{k}+\mathbf{K})\cdot\mathbf{r}} + \sum_{c} b_c \psi^{c}_{\mathbf{k}+\mathbf{K}}(\mathbf{r}) \right] \\
&= \sum_{\mathbf{K}} c_{\mathbf{K}} \left[e^{i(\mathbf{k}+\mathbf{K})\cdot\mathbf{r}} + \sum_{c} \left(- \int d\mathbf{r}'\, \psi^{c*}_{\mathbf{k}}(\mathbf{r}') e^{i\mathbf{k}\cdot\mathbf{r}'} \right) \psi^{c}_{\mathbf{k}+\mathbf{K}}(\mathbf{r}) \right] \\
&= \sum_{\mathbf{K}} c_{\mathbf{K}}\, e^{i(\mathbf{k}+\mathbf{K})\cdot\mathbf{r}} - \int d\mathbf{r}'\, \psi^{c*}_{\mathbf{k}}(\mathbf{r}') e^{i\mathbf{k}\cdot\mathbf{r}'} \sum_{\mathbf{K}} \sum_{c} c_{\mathbf{K}} \psi^{c}_{\mathbf{k}+\mathbf{K}}(\mathbf{r})
\end{aligned} \tag{3.59}$$

Now, using Bloch's theorem and the following expression:

$$\phi^{v}_{\mathbf{k}}(\mathbf{r}) = \sum_{\mathbf{k}} c_{\mathbf{K}}\, e^{i\mathbf{k}\cdot\mathbf{r}} \tag{3.60}$$

we promptly get [5, 42, 45]:

$$\psi^{v}_{\mathbf{k}}(\mathbf{r}) = \phi^{v}_{\mathbf{k}}(\mathbf{r}) - \sum_{c} \left[\int d\mathbf{r}'\, \psi^{c*}_{\mathbf{k}}(\mathbf{r}') \phi^{v}_{\mathbf{k}}(\mathbf{r}') \right] \psi^{c}_{\mathbf{k}}(\mathbf{r}) \tag{3.61}$$

Moreover, since $\psi^{v}_{\mathbf{k}}$ is an eigenstate of $\hat{\mathbf{H}}$, it must satisfy Schrödinger's equation with an eigenvalue ϵ^{v}_{k}, in other words:

$$H\psi^{v}_{\mathbf{k}} = \epsilon^{v}_{\mathbf{k}} \psi^{v}_{\mathbf{k}} \tag{3.62}$$

Consequently, if we plug 3.61 into 3.62, we find:

$$H\phi_{\mathbf{k}}^{v} - \sum_{c}\left(\int d\mathbf{r}'\,\psi_{\mathbf{r}}^{c*}\phi_{\mathbf{r}}^{v}\right) H\psi_{\mathbf{k}}^{c} = \epsilon_{\mathbf{k}}^{v}\left[\phi_{\mathbf{k}}^{v} - \sum_{c}\left(\int d\mathbf{r}'\,\psi_{\mathbf{k}}^{c*}\phi_{\mathbf{k}}^{v}\right)\psi_{\mathbf{k}}^{c}\right] \tag{3.63}$$

Finally, the same way as we had 3.62, we also have $H\psi_{\mathbf{k}}^{c} = \epsilon_{\mathbf{k}}^{c}\psi_{\mathbf{k}}^{c}$, which leads us to:

$$\begin{aligned} H\phi_{\mathbf{k}}^{v} - \sum_{c}\left(\int d\mathbf{r}'\,\psi_{\mathbf{r}}^{c*}\phi_{\mathbf{r}}^{v}\right)\epsilon_{\mathbf{k}}^{c}\psi_{\mathbf{k}}^{c} &= \epsilon_{\mathbf{k}}^{v}\left[\phi_{\mathbf{k}}^{v} - \sum_{c}\left(\int d\mathbf{r}'\,\psi_{\mathbf{k}}^{c*}\phi_{\mathbf{k}}^{v}\right)\psi_{\mathbf{k}}^{c}\right] \\ H\phi_{\mathbf{k}}^{v} &= \epsilon_{\mathbf{k}}^{v}\phi_{\mathbf{k}}^{v} - \epsilon_{\mathbf{k}}^{v}\sum_{c}\left(\int d\mathbf{r}'\,\psi_{\mathbf{k}}^{c*}\phi_{\mathbf{k}}^{v}\right)\psi_{\mathbf{k}}^{c} + \sum_{c}\left(\int d\mathbf{r}'\,\psi_{\mathbf{r}}^{c*}\phi_{\mathbf{r}}^{v}\right)\epsilon_{\mathbf{k}}^{c}\psi_{\mathbf{k}}^{c} \\ H\phi_{\mathbf{k}}^{v} &= \epsilon_{\mathbf{k}}^{v}\phi_{\mathbf{k}}^{v} + \sum_{c}(\epsilon_{\mathbf{k}}^{c} - \epsilon_{\mathbf{k}}^{v})\left(\int d\mathbf{r}'\,\psi_{\mathbf{k}}^{c*}\phi_{\mathbf{k}}^{v}\right)\psi_{\mathbf{k}}^{c} \end{aligned} \tag{3.64}$$

or simply:

$$(H + V_R)\,\phi_{\mathbf{k}}^{v} = \epsilon_{\mathbf{k}}^{v}\phi_{\mathbf{k}}^{v} \tag{3.65}$$

where

$$V_R = \sum_{c}(\epsilon_{\mathbf{k}}^{v} - \epsilon_{\mathbf{k}}^{c})\left(\int d\mathbf{r}'\,\psi_{\mathbf{k}}^{c*}\phi_{\mathbf{k}}^{v}\right)\psi_{\mathbf{k}}^{c} \tag{3.66}$$

Wherefrom we define the pseudopotential as the sum of the real potential, U, with V_R:

$$V_{pseudo} = -\frac{i\hbar^2}{2m}\nabla^2 + V_R \tag{3.67}$$

A handy note could be made in what concerns some consequences of 3.66. First note that 3.66 can be rewritten as follows:

$$V_R = \sum_{c}(\epsilon_{\mathbf{k}}^{v} - \epsilon_{\mathbf{k}}^{c})\left|\int d\mathbf{r}\,\psi_{\mathbf{k}}^{c*}\psi\right|^2 \tag{3.68}$$

Therefrom, once absolute values are always positive and $|\epsilon_{\mathbf{k}}^{c}| > |\epsilon_{\mathbf{k}}^{v}|$, we have that V_R always stands for a negative value. Consequently, the higher it is, the lower our potential will be and the closer we will be to doing free electron calculations for $\phi_{\mathbf{k}}^{v}$. On the other hand, since it depends on the energy of the level we are studying, basic theorems, such as the orthogonality of eigenfunctions belonging to different eigenvalues, are no longer applicable to H_{pseudo}.

Regarding pseudopotentials, many other approaches have been made in the past decades. They are mostly related to [42]:

- Pseudofunctions without nodes;
- Eigenvalues for valence states are equal to the ones gotten with the pseudopotential;
- The pseudofunction and the real wave function of all electrons must be equal from a specified cutoff radius r_c;
- The electronic charge within the region delimited by r_c must be equal for both, the pseudofunction R^{PS} and for the *all electron* function R_l^{AE};
- The logarithmic derivation of the wavefunction and the *all electron* function must be equal to each at $r = r_c$;

3.5.3 Ultrasoft Pseudopotentials

Most methods we have discussed so far handle fairly well many elements and, in particular, paved the way to perform accurate calculations of electronic systems within the local density approximation using plane waves. Despite that, we would still find a hard time if we applied them straightforwardly to crystals with highly localized valence orbitals because they are still spanned by a very large set of plane waves, which implies directly into a huge computational cost. Luckily, we can overcome this issue through ultrasoft pseudopotentials, as proposed by Vanderbilt in 1990 [42].

Vanderbilt proposed replacing the standard pseudopotentials with one that had the following properties [55]:

- Takes on the form of a sum of a few separable items;
- Becomes local and vanishes outside the core;
- It is differentiable;
- The norm-conserving constraint is removed;
- It is involved in screening processes;

In short, it allows us to increase the cutoff radius without sacrificing transferability.

3.5.4 *All electrons* method

This method involves a spatial breakdown into two distinct regions: the core, housing all inner electrons, and the valence region. In the core region, atomic characteristics dominate and strongly influence all behaviors. Consequently, the solutions in this realm are obtained using spherical harmonics the same way as we do for Hydrogen and, in a first approach, for Helium. On the other hand, in the valence region, once the potential doesn't vary heavily anymore, all solutions are determined using plane waves. Besides, it is essential to consider constraints related to the differentiation and continuity of solutions throughout the entire spatial domain, particularly in the boundary regions, otherwise, the solutions would just be unacceptable [17]. These considerations led to the development of the augmented plane waves (APW) basis. This method was developed by Slater in 1965 but wasn't used for years due to its high computational cost regarding the solution within the inner region [42].

It puts an end to our discussion about assembling a numerical method to study crystals. We have gone over all the essential theories and briefly pointed out some possible changes to consider more greatnesses such as the spin, excited states, or even all electrons. In the upcoming chapter, we will briefly review our main objectives and present both our results and findings.

Chapter 4

Results

Before any words regarding all acquired results, it is worth pointing out that the current work is a byproduct of previous collaborations of my advisor, Wendel S. Paz, who constructed the base and guided me through all the following results. Besides, as aforementioned, to directly detect a new particle, we are mainly interested in measuring an observable effect out of its interaction with a target [30]. Then, the issue now is: what should this target look like? Regarding light-dark matter, we should search for a material that satisfies the following points [24, 49]:

- It must be scalable;
- It must be a semiconductor;
- Its Fermi velocity must be of the order of $10^{-3}c$;
- It must be a topological insulator;

Lastly, from previous papers published by my advisor [37, 58], we knew that Samarium Hexaboride, SmB_6, had a strong chance of satisfying all those items since it was already known that it had surface-protected states and a flatter valence band. Thus, from that point on, we intended to bring up and double-check previous results and further discuss its Fermi velocity and topology.

In what follows, we will perform some convergence tests to find the cut-off parameters that return an acceptable computation cost, find the most stable structure from a theoretical point of view, and check whether SmB_6 satisfies the points stated above.

4.1 Convergence Tests

Our first step in performing a theoretical study of a new material, by standard, consists of establishing its spatial configuration and all cut-off parameters responsible for breaking down the auto-consistent cycle when one of them is exceeded. Doing so, we will be shown a set of parameters that safely depict the material from a theoretical point of view and also prevent us from doing overwork. Before jumping to results, though, it is worth noting that regarding its structure, we employed the following figure and values for its primitive cell and atomic positions, respectively.

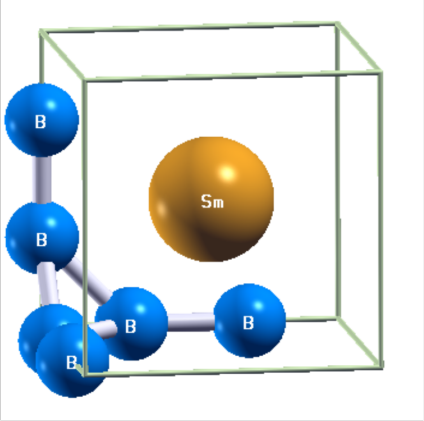

Figure 4.1. SmB_6 primitive cell.

Table 4.1. Atomic Positions

Atom	x (a_0)	y (a_0)	z (a_0)
Sm	2.059003078	2.059003078	2.059003078
B	0.000000000	0.000000000	1.238936725
B	0.000000000	0.000000000	2.879069430
B	1.238936725	0.000000000	0.000000000
B	2.879069430	0.000000000	0.000000000
B	0.000000000	1.238936725	0.000000000
B	0.000000000	2.879069430	0.000000000

Besides, we performed all auto-consistent calculations with the aid of the script shown in appendix A.1. Employing it within a for-loop, with a lace-variable help, we managed to find all cut-off

parameters by varying the desired greatnesses over a beforehand set range. This way, we varied each parameter at a time and plotted it on a *Total Energy* $\times$ *variable graph*. Finally, we stepped into the problem of getting the cut-off parameters by calculating first the cut-off energy, E_{cut}. It is still worth noting that even though a precise theoretical value for the lattice constant is missing, we had to set it up beforehand to find out E_{cut}. Then, assuming $a \approx 4.13\,\text{Å}$, which was an experimental value found for SmB_6 lattice constant [10], we obtained the following relationship between E_{cut}[1] and the total energy, E_{tot}:

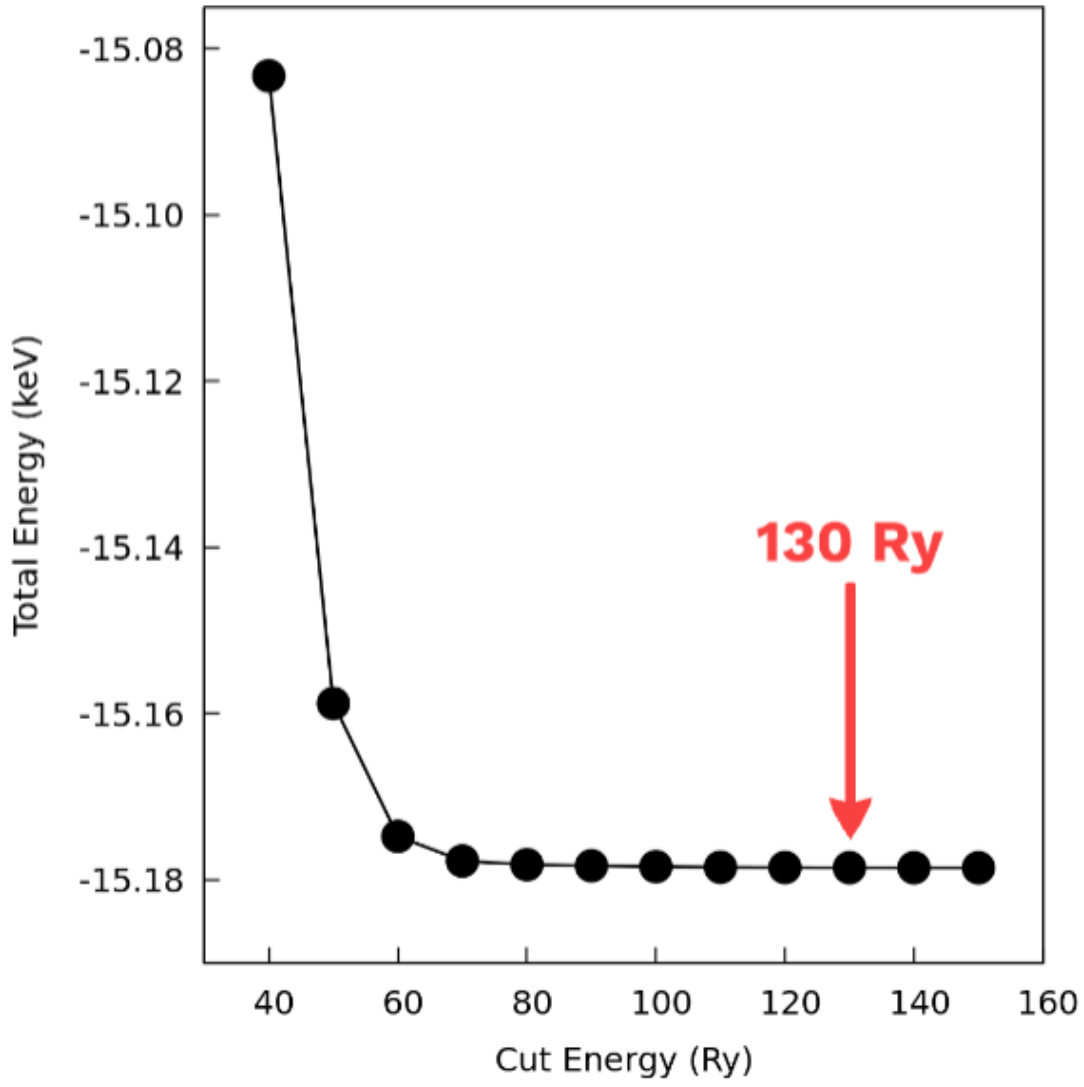

Figure 4.2. Variation of the total energy of the system according to the chosen E_{cut}.

[1] It is important to note that E_{cut} is directly related to the number of plane waves necessary to span all the electronic states [42].

From this figure, we can promptly observe that any E_{cut} within the range that goes from 80 Ry up to 160 Ry returns the same total energy for the system. On the other hand, the higher it is, the more computational cost these calculations have. Anyway, since our system was fairly simple, we chose the value of 130 Ry for E_{cut} as pointed out in the chart. This value is in between the mentioned limits and gives us some freedom to add other features to the system later. In what follows, we searched for the number of k points that best described the system with an acceptable computational cost. This way, employing a Monkhorst-Pack mesh and following the same steps as before, we varied the number of occupied k-sites and calculated the related E_{tot}, finally reaching the following relationship between E_{tot} and $k\ points$:

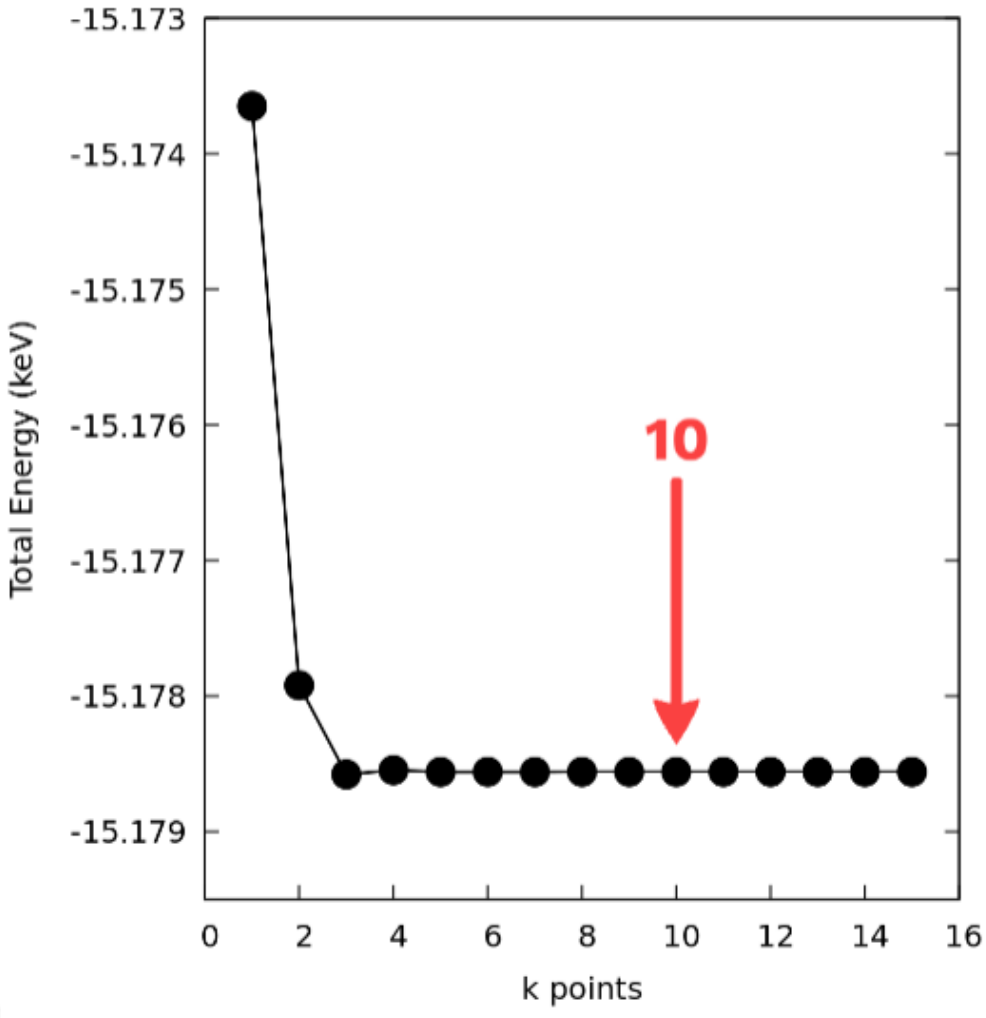

Figure 4.3. Relationship between the total energy of the system and the Monkhorst-Pack mesh chosen.

It can be seen from this graph that there is almost no change in E_{tot} when k becomes greater than 4. On the other hand, since a 4 x 4 x 4 mesh usually has a very low computational cost and our system has to take symmetries and spin-orbit effects into consideration, we employed a 10 x 10 x 10 mesh instead. Lastly, employing everything we have found so far, we calculated the theoretical lattice constant that made E_{tot} the least. Doing so, we found the following relationship between the lattice constant and E_{tot}:

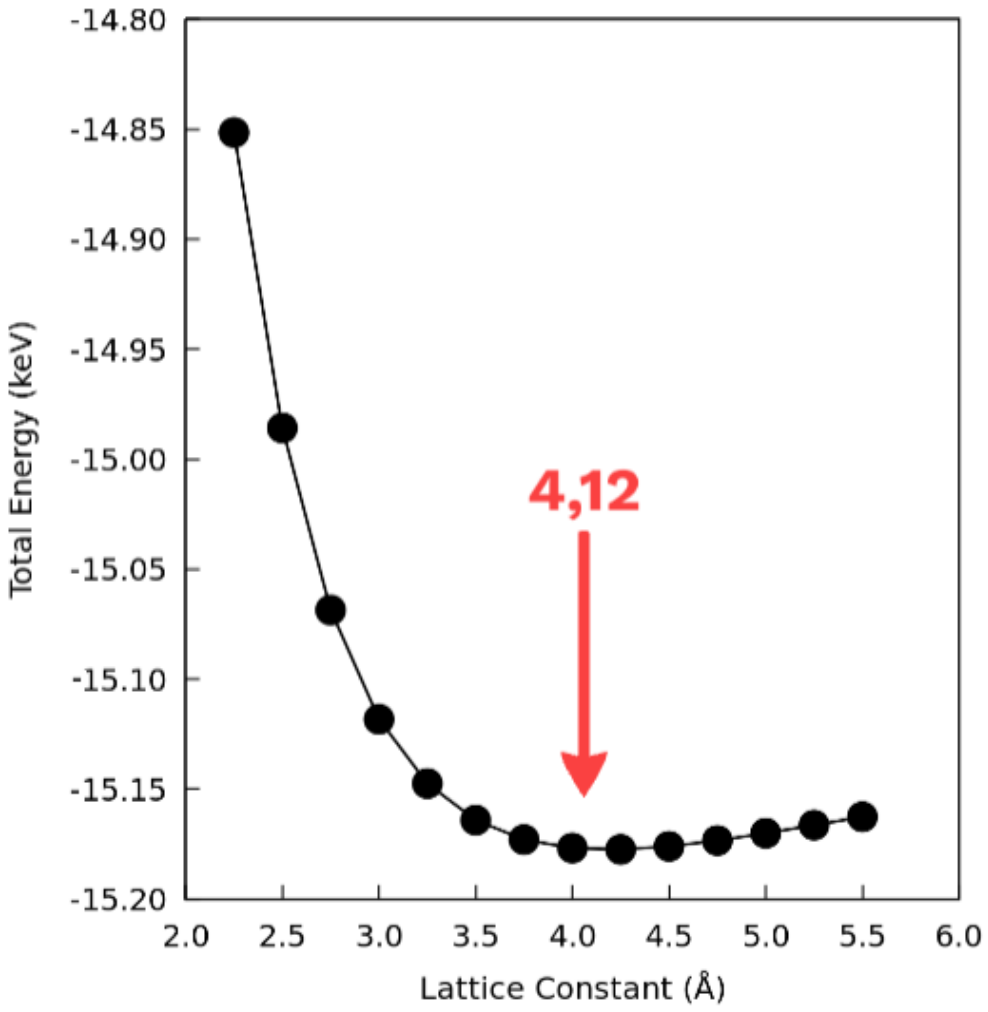

Figure 4.4. Variation of the total energy of the system according to the chosen lattice constant. It can be seen that, as expected, there is a global minimum on the graph over $a = 4.118\,\text{Å}$, which stands for the most stable structure.

From this, we got that the lattice constant is approximately $4.118\,\text{Å}$, which stands for a numerical error of 1.2 % from the experimental value found in [10].

4.2 SmB_6 Band Structure

To calculate the band structure of SmB_6, we opened the file displayed in A.1 on Xcrysden, chose a path within its Wigner-Seitz cell, replaced the Monkhorst-Pack mesh with the given points for k, which were simply the high-symmetry points of its Wigner-Seitz cell, and changed the calculation mode from 'scf' to 'bands'[2]. Then, employing the post-processing package bands.x [6], we managed to find its band structure. Its band structure as well as some of the high symmetry points employed are shown below.

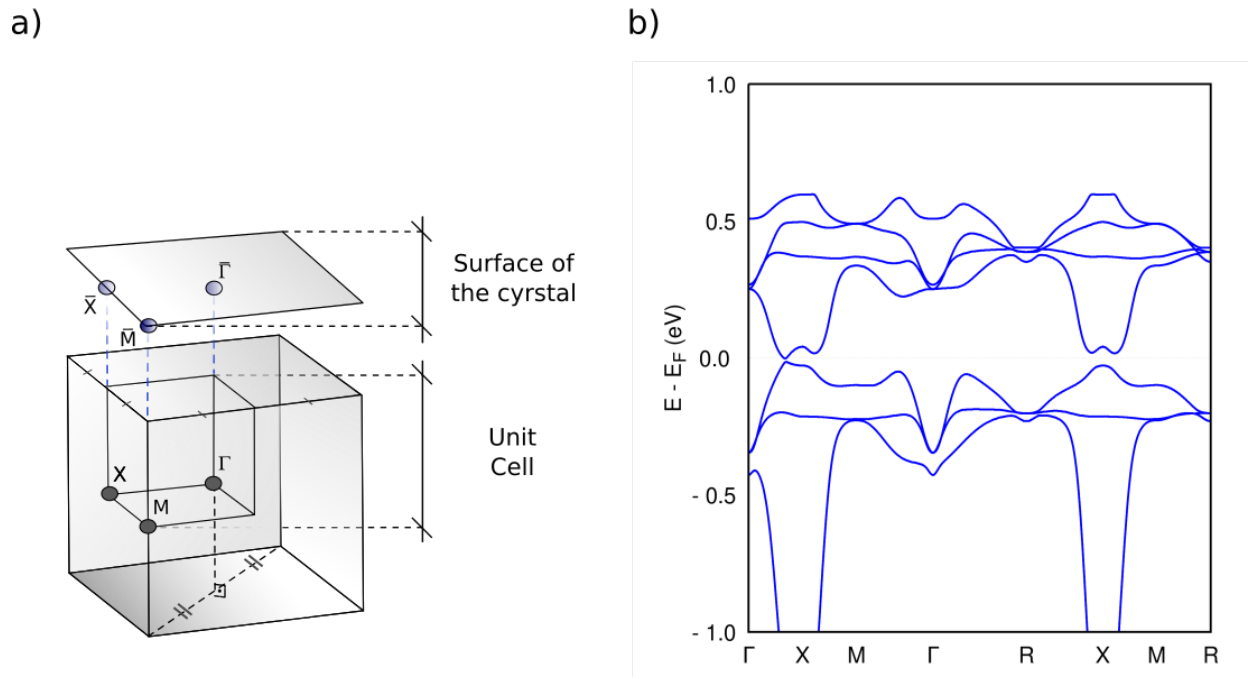

Figure 4.5. a) High symmetry points in the SmB_6 Wigner-Seitz cell. b) Plain band structure of SmB_6 *bulk*.

From this, we got that the gap energy along the ΓXM path was 12.5 meV, which is consistent with former results found in [29] and [37].

[2] A further discussion about the full procedure followed here may be found in [6].

4.3 Fermi Velocity

To calculate its Fermi velocity, we employed the development shown in the overview. At this point, it is worth recalling that we have three different ways of getting the derivations in:

$$m^* = \frac{\hbar^2}{\frac{\partial^2 E}{\partial k^2}} \quad , \quad m^* = \frac{\hbar^2}{\frac{\partial^2 E}{\partial k_\alpha \partial k \beta}} \tag{4.1}$$

they are analytically, numerically, or through approximations, in which we would use a well-known function to parameterize the region of interest, which is the surrounding area where the optical transition is taking place. In the current work, since the output given by Quantum Espresso isn't analytic, we employed the last two, but once many $k\ points$ were identical within the software accuracy, we found a hard time trying to perform the derivations while avoiding infinities and not changing the data itself, so we preferred to use an approximation at this stage. In this case, since we are only interested in the region where the optical transition takes place, and this one is smooth, we opted to use a harmonic function. All subsequent steps were taken using Gnuplot.

4.3.1 Validity of Harmonic Approximation

Before stepping into SmB_6, though, we first performed a test on germanium bulk employing some data shared by our research group. Then, since its Fermi surface is symmetric around the optical transition point, we fell into the first of the two cases shown in 4.1. Consequently, we are in 2D and, instead of a tensor, we used the following expression to find m^*:

$$m^* = \frac{\hbar^2}{\frac{\partial^2 E}{\partial k^2}} \tag{4.2}$$

Its band structure and harmonic approximation are presented in figure 4.6.

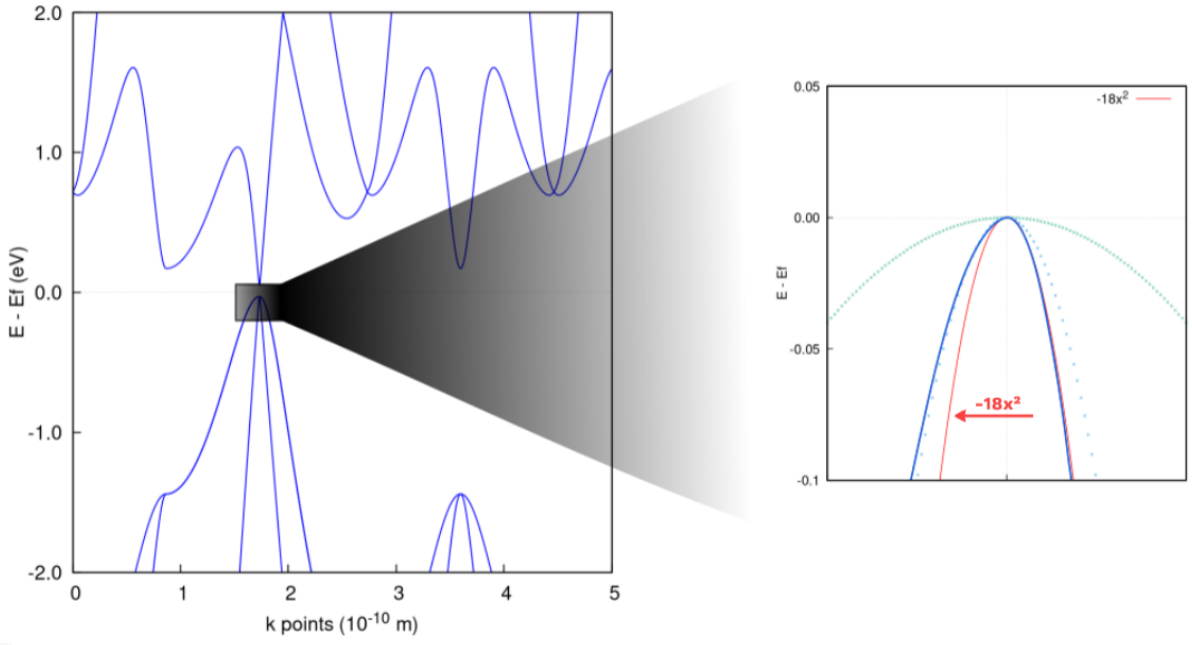

Figure 4.6. Band structure of Germanium bulk and some harmonic approximations for the valence band around the optical transition point. Here, as outlined on the graph, the function that made the best fit was $E(k) = -18\,k^2$.

Then, if we plug the found function, $E(k) = -18k^2$, in 4.1, we find:

$$m^* = \frac{\hbar^2}{\frac{\partial^2}{\partial k^2}\left[18k^2 \cdot (1.609 \cdot 10^{-19}) \cdot (10^{-20})\right]} \approx 1.91 \cdot 10^{-31}\ \text{kg} \approx 0.21\ m_e \tag{4.3}$$

where m_e stands for the mass of the electron. Note that we have also employed two other constants to translate our units into the SI system and end up with kilograms. Lastly, it precisely corresponds to the values found in [35] and [57]. Consequently, we can safely employ this procedure to SmB_6.

4.3.2 SmB_6 Fermi Velocity

In what follows, our first step was to analyze whether there was isotropy or not around the optical transition point. To check that, we analyzed the Fermi surface presented in figure 4.7.

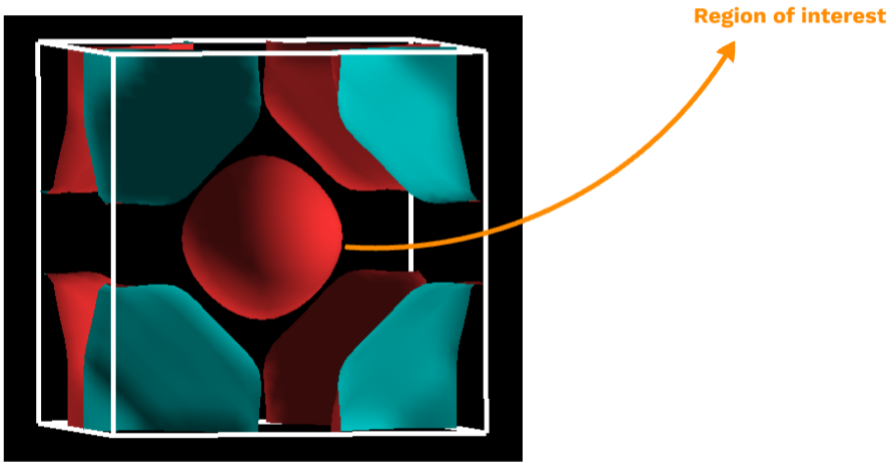

Figure 4.7. Fermi surface of SmB_6 valence band.

Since its core, which stands for the region of interest, is isotropic, we fell into the same spot as before and could follow the same steps as though we were handling germanium again. Keeping that in mind, we cut off the last (44th band) and first (45th band) valence and conduction bands, respectively, over the region $\Gamma X M$. Therefrom, we looked for the harmonic function that fitted the valence band best. These steps are depicted in figure 4.8.

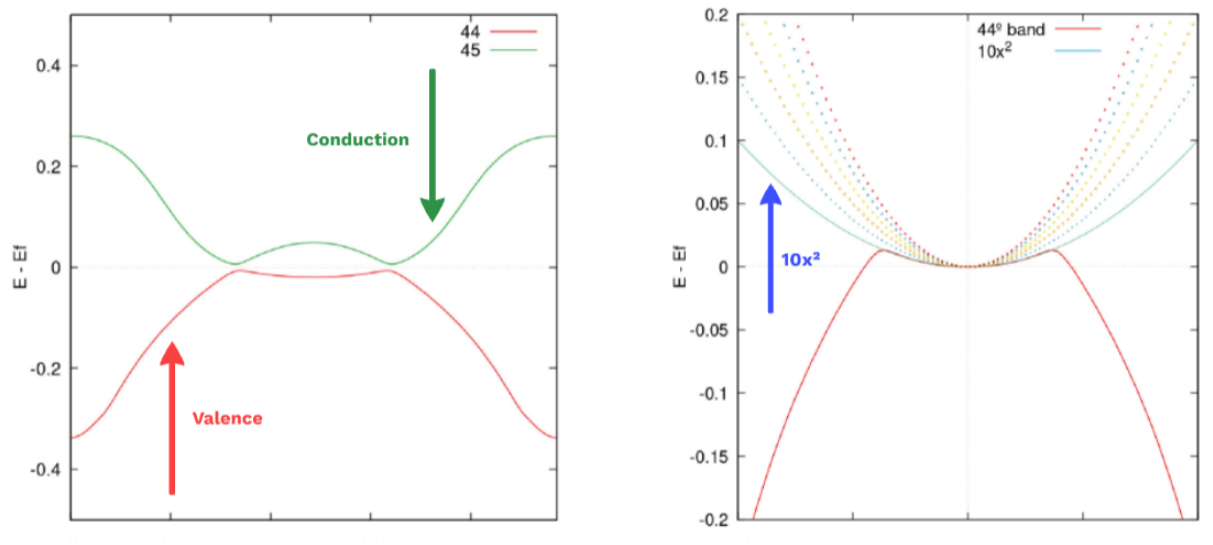

Figure 4.8. On the left, it is shown the last valence and the first conduction band of SmB_6 bulk, while on the right it was performed some harmonic approximations for the valence band around the optical transition point. Here, as outlined on the graph, the function that made the best fit was $E(k) = 10\,k^2$.

Thus, employing the found function, $E(k) = 10k^2$, we got:

$$m^* = \frac{\hbar^2}{\frac{\partial^2}{\partial x^2}\left[10k^2 \cdot (1.609 \cdot 10^{-19}) \cdot (10^{-20})\right]} \approx 3.456 \cdot 10^{-31}\ \text{kg} \approx 0.380\ m_e \tag{4.4}$$

and then, for its Fermi velocity, we found:

$$\text{v}_f = \frac{\hbar \text{k}}{m^*} = \frac{(1.0545 \cdot 10^{-34}) \cdot (0.0850 \cdot 10^{10})}{3.456 \cdot 10^{-31}} \approx 259,353,299\ \text{m/s} \approx 8.651 \cdot 10^{-4}\,\text{c} \tag{4.5}$$

where we got the $k\ point$ from the band structure output. It stands for the highest point of the valence band.

4.4 Indicative of a non-trivial Topology

Using the Quantum Espresso function projwfc.x [26, 46], we projected the found band structure onto the atomic orthogonalized orbitals s, p, d, and f. By doing so, we were able to precisely analyze whether there were any band inversions or not. The final graphs are presented below.

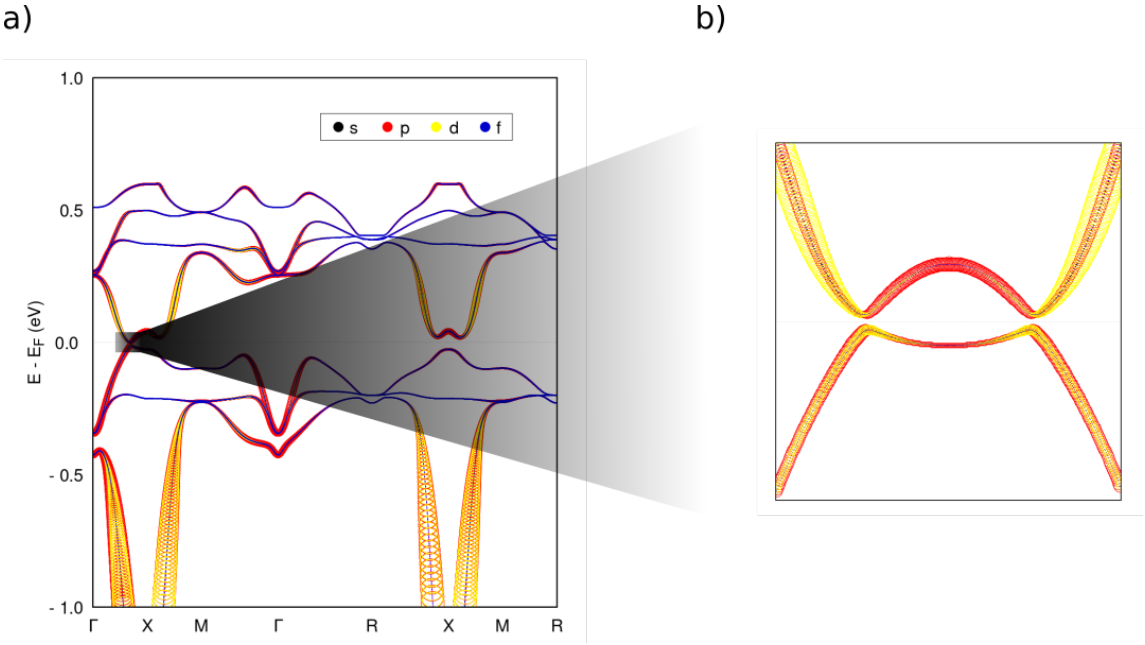

Figure 4.9. a) Projection of SmB_6 onto the atomic orthogonalized orbitals s, p, d, and f. b) Cut of the region where a band inversion is taking place. Note how the behavior of the valence band is being transferred to the conduction band and inversely. That precisely characterizes a band inversion and is strong evidence that the material has a non-trivial topology.

It is important to note, though, that since SmB_6 is a highly correlated material, there was found a massive predominance of the orbital f in the region of interest, which we had to carefully soften with the following weights so we could properly observe those band inversions:

$$s = 0.05 \quad , \quad p = 0.03 \quad , \quad d = 0.1 \quad , \quad f = 0.00003 \tag{4.6}$$

That interchange in the orbitals between the valence and conduction bands is a high indication that the material does not have a trivial topology, being then a topological insulator. Unfortunately, that is not enough to classify it as such, still requiring either an experimental verification, an analysis of its berry phase, or a study of its surface states.

4.5 Review

In short, we found that Samarium Hexaboride had the following properties:

- It is a semiconductor with a 12.5 meV gap along the ΓXM path;
- Its Fermi velocity is of the order of 10^{-3} c;
- Due to a band inversion between the last valence and the first conduction bands, it possibly has non-trivial topology;

Chapter 5

Conclusion

In the pursuit of understanding what properties a material should satisfy to be employed in detecting light-dark matter (LDM) particles, this dissertation aimed to give some special attention to Samarium Hexaboride (SmB_6). Throughout the investigation, the focus remained on its band gap, scalability, Fermi velocity, and topology. As the findings presented in this study unfold, they shed light on the significance of detecting LDM particles as a way to reach a higher level of understanding of the universe, confirming the relevance and importance of this inquiry by proposing SmB_6 as a possible target.

The culmination of this research has brought forth several noteworthy findings, they are:

- SmB_6 is a semiconductor with a band gap given by 12.5 meV;
- We can produce a polycrystalline powder using molten salt electrolysis. In what follows, we can grow the crystal using the flux method. The properties of the crystal depend on the method employed in its growth process, though;
- Its Fermi velocity is of the order of $10^{-3}\,c$;
- It has a non-trivial topology, having then surface-protected states;

These findings collectively allow us to address the question of whether the current material has all the required properties to be employed as a target in detecting LDM particles directly or not. Regarding the articles [20, 24, 30, 49], we can positively answer the aforementioned inquiry, SmB_6 satisfies all requirements according to the direct detection model adopted. This synthesis not only

answers the initial research questions but also sheds light on valuable inquiries about what other materials could be used in this hunting.

Even though we have reached valuable findings regarding SmB_6, the probability of interaction between LDM particles and our target is pretty low on Earth. Consequently, regarding the detection experiment, we still have to find out how we could bypass the problem of detecting a single interaction between LDM and SmB_6. Despite that, another possibility is to continue our research for other materials that also satisfy all requirements for being employed as targets.

Appendix A

Computational Methods

All calculations on this work were performed on Quantum Espresso employing one of the following methods[1]: pw.x, bands.x, projwfc.x. Besides, the standard functional employed here was a GGA within the Perdew-Burke-Ernzerhof (PBE) formalism [43]. Lastly, Quantum Espresso is a highly reliable software that works with plane waves, which, even though a high computational cost rises when dealing with vacuums, is the main reason why we opted to work with it.

A.1 Inputs

Below is shown the main code employed in performing all convergence tests as well as finding SmB_6 properties. It follows Quantum Espresso syntax and further information may be found in [16].

A.1.1 Self-consistent field (scf) input code

&CONTROL
calculation = 'scf'
verbosity = 'high'
restart_mode = 'restart'
nstep = 150
tstress = .true.
tprnfor = .true.
prefix = 'SmB6'
etot_conv_thr = 1.0D-5
forc_conv_thr = 1.0D-3

[1] Further information may be found on [6] and [46].

```
pseudo_dir = '/packages/pseudo/'
outdir = '/scratch/thiago/scr/'
/

&SYSTEM
ibrav = 0
a = 1.0
nat = 7
ntyp = 2
ecutwfc = 130
ecutrho = 530
nspin = 1
noncolin = .true.
lspinorb = .true.
occupations ='fixed'
nbnd = 52
! vdw_corr ='grimme-d2'
smearing ='gaussian'
degauss = 0.002
/

&ELECTRONS
electron_maxstep = 300
conv_thr = 1.0d-9
diagonalization ='david'
mixing_mode = 'plain'
mixing_beta = 0.3
/

&IONS
ion_dynamics = 'bfgs'
/

&CELL
cell_dynamics ='bfgs'
cell_factor = 3.0D0
cell_dofree = all
/

ATOMIC_SPECIES
Sm 150.36 Sm.rel-pbe-spdfn-kjpaw_psl.1.0.0.UPF
B 10.81 B.rel-pbe-n-kjpaw_psl.1.0.0.UPF

ATOMIC_POSITIONS
Sm 2.059003078 2.059003078 2.059003078
B 0.000000000 -0.000000000 1.238936725
B 0.000000000 0.000000000 2.879069430
B 1.238936725 0.000000000 -0.000000000
B 2.879069430 -0.000000000 -0.000000000
B 0.000000000 1.238936725 0.000000000
B 0.000000000 2.879069430 -0.000000000

CELL_PARAMETERS {alat}
4.118006155 0.000000000 0.000000000
0.000000000 4.118006155 0.000000000
0.000000000 0.000000000 4.118006155

K_POINTS {automatic}
10 10 10 0 0 0
```

A.2 Figures and Other Methods

All pictures were generated using one or a set of the following software: Xcrysden, Gnuplot, Vesta, Prezi, or Inkscape. The cut-bands shown in figure 4.8, as well as their harmonic approximations, were obtained through a plain bash code [19, 38] whose output was processed on Gnuplot afterward.

Bibliography

[1] Andernach, H. and Zwicky, F. "English and Spanish Translation of Zwicky's (1933) The Redshift of Extragalactic Nebulae". In: *arXiv preprint arXiv:1711.01693* (2017).

[2] Ando, Y. "Topological Insulator Materials". In: *Journal of the Physical Society of Japan* 82 (2013), pp. 1–32. DOI: 10.7566/JPSJ.82.102001. URL: https://journals.jps.jp/doi/epdf/10.7566/JPSJ.82.102001.

[3] Arfken, G. B. and Weber, H. J. *Mathematical Methods for Physicists*. Elsevier, 2005. ISBN: 9780120598762.

[4] Ariel, V. and Natan, A. *Electron Effective Mass in Graphene*. 2012. arXiv: 1206.6100 [physics.gen-ph].

[5] Ashcroft, N. W. and Mermim, N. D. *Solid State Physics*. New York: Harcourt College Publishers, 1976. ISBN: 0-03-083993-9.

[6] *Bandstructure Calculation*. Guide about how to calculate band structures on Quantum Espresso with examples. Accessed on 05.12.2023. URL: https://pranabdas.github.io/espresso/hands-on/bands/.

[7] Batista, N. N. "Estudo Teórico de Transições de Fase Topológica na Franqueita: Uma heteroestrutura de van der Waals de Formação Natural". MA thesis. UFES, 2021.

[8] Berchmans, L. J. et al. "Electrosynthesis of Samarium Hexaboride using tetra borate melt". In: *Ionics* 16 (2010), pp. 833–838. DOI: 10.1007/s11581-010-0469-3. URL: https://link.springer.com/article/10.1007/s11581-010-0469-3#citeas.

[9] Born, M. and Oppenheimer, R. "Zur Quantentheorie der Molekein". In: *Annalen Der Physik* 23.10 (1927), pp. 457–484. DOI: 10.1002/andp.19273892002.

[10] Cahill, J. T. and Graeve, O. A. "Hexaborides: a review of structure, synthesis and processing". In: *Journal of Materials Research and Technology* 8.6 (2019), pp. 6321–6335. ISSN: 2238-7854. DOI: https://doi.org/10.1016/j.jmrt.2019.09.041. URL: https://www.sciencedirect.com/science/article/pii/S2238785418311062.

[11] Castellani, O. C. "Discussão dos Conceitos de Massa Inercial e Massa Gravitacional". In: *Revista Brasileira de Ensino de Física* 23.3 (2001), pp. 356–359. DOI: 10.1590/S1806-11172001000300013.

[12] Ceperly, D. M. and Alder, B. J. "Ground State of the Electron Gas by a Stochastic Method". In: *Physical Review Letters* 45.7 (1980), pp. 566–569. DOI: 10.1103/physrevlett.45.566.

[13] Cohen-Tannoudji, C., Diu, B., and Laloë, F. *Quantum Mechanics*. Vol. 1. Wiley-VCH, 2020. ISBN: 978-3-527-34553-3.

[14] Cohen-Tannoudji, C., Diu, B., and Laloë, F. *Quantum Mechanics*. Vol. 2. Wiley-VCH, 2020. ISBN: 978-3-527-34554-0.

[15] Curtiss, A. et al. "Gaussian-1 theory of molecular energies for second-row compounds". In: *AIP — The Journal of Chemical Physics* 93.4 (1990), pp. 2537–2545. DOI: 10.1063/1.458892.

[16] *Density Functional Theory using Quantum Espresso*. Guide about Quantum Espresso usage with examples. Accessed on 05.12.2023. URL: https://pranabdas.github.io/espresso/.

[17] Eisberg, R. and Resnick, R. *Física Quântica: Átomos, Moléculas, Sólidos, Núcleos e Partículas*. Vol. 1. Campus, 1979. ISBN: 8570013094.

[18] *Eletrólise*. Lecture, Department of Chemistry, Universidade de São Paulo, São Paulo, SP, Brazil. http://tinyurl.com/72sadawy. Accessed on 21.12.2023.

[19] Garrels, M. *Bash Guide for Beginners*. Accessed on 05.12.2023. URL: https://tldp.org/LDP/Bash-Beginners-Guide/Bash-Beginners-Guide.pdf.

[20] Geilhufe, R. Matthias et al. "Materials Informatics for Dark Matter Detection". In: *physica status solidi (RRL) – Rapid Research Letters* 12.11 (Sept. 2018). ISSN: 1862-6270. DOI: 10.1002/pssr.201800293. URL: http://dx.doi.org/10.1002/pssr.201800293.

[21] Giustino, F. *Materials Modeling using Density Functional Theory: Properties & Predictions*. Oxford, 2014. ISBN: 978–0–19–966244–9.

[22] Grebenkemper, J. *Powder X-ray Diffraction*. Accessed on 05.12.2023. URL: https://chem.libretexts.org/Bookshelves/Analytical_Chemistry/Supplemental_Modules_(Analytical_Chemistry)/Instrumentation_and_Analysis/Diffraction_Scattering_Techniques/Powder_X-ray_Diffraction/.

[23] Griffiths, D. *Introduction to Electrodynamics*. Prentice Hall, 1999. ISBN: 0-13-805326-X.

[24] Hochberg, Y. et al. "Detection of sub-MeV Dark Matter with Three-dimensional Dirac Materials". In: *Physical Review D* 97 (2018), pp. 1–24. DOI: 10.1103/PhysRevD.97.015004. URL: https://journals.aps.org/prd/abstract/10.1103/PhysRevD.97.015004.

[25] Hohenberg, P. and Kohn, W. "Inhomogeneous Electron Gas*". In: *Physical Review* 136.3B (1964), B864–B871. DOI: 10.1103/PhysRev.136.B864.

[26] *Input File Description*. Manual of projwfc.x with all its keywords. Accessed on 05.12.2023. URL: https://www.quantum-espresso.org/Doc/INPUT_PROJWFC.html.

[27] Jaeger, G. "The Ehrenfest Classification of Phase Transitions: Introduction and Evolution". In: *Archive for History of Exact Sciences* 53 (1998), pp. 51–81. DOI: 10.1007/s004070050021.

[28] Janak, J. F. "Proof that $\delta E/\delta \eta_i = \epsilon_i$ in density-functional theory". In: *Physical Review B* 18.12 (1978), pp. 7165–7168. DOI: 10.1103/PhysRevB.18.7165.

[29] Kang, C., Kim, J., Kim, K., et al. "Band Symmetries of Mixed-Valence Topological Insulator: SmB6". In: *Journal of the Physical Society of Japan* 84.024722 (2015), pp. 1–7. DOI: 10.7566/JPSJ.84.024722.

[30] Klasen, M., Pohl, M., and Sigl, G. "Indirect and Direct Search for Dark Matter". In: *Progress in Particle and Nuclear Physics* 85 (2015), pp. 1–32. ISSN: 0146-6410. DOI: https://doi.org/10.1016/j.ppnp.2015.07.001. URL: https://www.sciencedirect.com/science/article/pii/S0146641015000460.

[31] Kohn, W. and Sham, L. J. "Quantum Density Oscillations in an Inhomogeneous Electron Gas*". In: *Physical Review* 137.6A (1965), A1697–A1705. DOI: 10.1103/PhysRev.137.A1697.

[32] Kohn, W. and Sham, L. J. "Self-consistent Equations Including Exchange and Correlation Effects*". In: *Physical Review* 140.4A (1965), A1133–A1138. DOI: 10.1103/PhysRev.140.A1133.

[33] Lemos, N. A. *Mecânica Analítica*. Editora Livraria da Física, 2007. ISBN: 9788588325241.

[34] Li, L., Sun, K., Kurdak, C., et al. "Emergent mystery in the Kondo insulator samarium hexaboride". In: *Nature Review Physics* 2 (2020), pp. 463–479. DOI: 10.1038/s42254-020-0210-8.

[35] Ma, I, Zhang, H., Wang, X., et al. "Valence band structure and hole effective mass of uniaxial stressed Germanium". In: *Journal of Computational Electronics* 10 (2011), pp. 388–393. DOI: 10.1007/s10825-011-0374-7.

[36] Majumdar, D. *Dark Matter: An Introduction*. Boca Raton: CRC Press, 2014. ISBN: 9780429101472.

[37] Matt, C. E. et al. "Consistency between ARPES and STM measurements on SmB_6". In: *Physical Review B* 101 (8 Feb. 2020), p. 085142. DOI: 10.1103/PhysRevB.101.085142. URL: https://link.aps.org/doi/10.1103/PhysRevB.101.085142.

[38] Maziolli, G. *Guia Foca Linux*. Accessed on 05.12.2023. URL: https://guiafoca.org/guiaonline/iniciante/.

[39] Miller, Marli. *Rhombic Cleavage in Calcite*. Photo Gallery. https://geologypics.com/min-25/. Accessed on 21.12.2023. Apr. 2017.

[40] Nasa. *Galaxies*. Article. https://universe.nasa.gov/galaxies/large-scale-structures/. Accessed on 21.12.2023. 2004.

[41] Nasa. *Galaxies Over Time*. Article. https://science.nasa.gov/mission/webb/galaxies-over-time/. Accessed on 21.12.2023.

[42] Paz, W. S. "Estudo de Vacâncias em Grafeno via Cálculos de Primeiros Princípios". MA thesis. UFES, 2013. URL: http://repositorio.ufes.br/handle/10/7445.

[43] Perdew, J. P., Burke, K., and Ernzerhof, M. "Generalized Gradient Approximation Made Simple". In: *Physical Review Letters* 77.18 (1996), pp. 3865–3868. DOI: 10.1103/physrevlett.77.3865.

[44] Perdew, J. P. and Zunger, A. "Self-interaction correction to density-functional approximations for many-electron systems". In: *Physical Review B* 23.10 (1981), pp. 5048–5079. DOI: 10.1103/physrevb.23.5048.

[45] Phillips, J. C. and Kleinman, L. "Method for Calculating Wave Functions in Crystals and Molecules*". In: *Physical Review* 116.2 (1959), pp. 287–294. DOI: 10.1103/PhysRev.116.287.

[46] *Projected Density of States*. Guide about Quantum Espresso usage with examples. Accessed on 05.12.2023. URL: https://pranabdas.github.io/espresso/hands-on/pdos.

[47] Rappoport, D. et al. "Which functional should I choose?" In: *Encyclopedia of Inorganic Chemistry* (Sept. 2009). DOI: 10.1002/0470862106.ia615.

[48] Salinas, S. R. A. *Introdução à Física Estatística*. São Paulo: Edusp, 2008. ISBN: 9788531403866.

[49] Sánchez-Martínez, M-Á et al. "Spectral and optical properties of Ag3Au(Se2,Te2) and dark matter detection". In: *Journal of Physics: Materials* 3.1 (Oct. 2019), p. 014001. ISSN: 2515-7639. DOI: 10.1088/2515-7639/ab3ea2. URL: http://dx.doi.org/10.1088/2515-7639/ab3ea2.

[50] Sears, F. W. and Salinger, G. L. *Termodinâmica, Teoria Cinética e Termodinâmica Estatística*. Guanabara Dois S.A., 1979.

[51] Simon, S. H. *The Oxford Solid State Basics*. Oxford, 2013. ISBN: 978–0–19–968077–1.

[52] *Solid State Chemistry*. Lecture, Department of Chemistry, St. Joseph's College, Tiruchirappalli, TN, India. "https://www.sjctni.edu/Department/ch/eLecture/SolidState.pdf". Accessed on 05.12.2023. Sept. 2023.

[53] Thornton, S. T. and Marion, J. B. *Classical Dynamics of Particles and Systems*. Thomson Brooks/Cole, 2004. ISBN: 0-534-08378-1.

[54] Trzesniak, D. R. F. "Modelagem quântica de inibidores enzimáticos". MA thesis. USP, 2002. URL: https://doi.org/10.11606/D.43.2002.tde-26062002-143722.

[55] Vanderbilt, D. "Optimally smooth norm-conserving pseudopotentials". In: *Physical Review B* 32.12 (1985), pp. 8412–8415. DOI: 10.1103/PhysRevB.32.8412.

[56] Watari, K. and Fazzio, A. *Introdução À Teoria de Grupos Aplicada Em Moléculas e Sólidos*. UFSM, 2009. ISBN: 9788573911114.

[57] Zeebroeck, B. J. V. *Effective mass in semiconductors*. Lecture, Department of Physics, Mid Sweden University, Sweden. 1997. URL: http://apachepersonal.miun.se/~gorthu/halvledare/Effective%20mass%20in%20semiconductors.htm.

[58] Zhixiang, S., Maldonado, A., Paz, W. S., et al. "Observation of a well-defined hybridization gap and in-gap states on the SmB_6 (001) surface". In: *Physical Review B* 97 (23 June 2018), p. 235107. DOI: 10.1103/PhysRevB.97.235107. URL: https://link.aps.org/doi/10.1103/PhysRevB.97.235107.